Naval Research Laboratory
Washington, DC 20375-5320

NRL/MR/6707--94-7444

(2)

Gyrotrons and Free Electron Lasers for Atmospheric Sensing

WALLACE M. MANHEIMER

Senior Scientist Fundamental Plasma Processes
Plasma Physics Division

February 28, 1994

REPORT DOCUMENTATION PAGE

Form Approved
OMB No. 0704-0188

1. AGENCY USE ONLY *(Leave Blank)*	2. REPORT DATE	3. REPORT TYPE AND DATES COVERED
	February 28, 1994	Interim

4. TITLE AND SUBTITLE

Gyrotrons and Free Electron Lasers for Atmospheric Sensing

5. FUNDING NUMBERS

PE - 61153N

6. AUTHOR(S)

W. M. Manheimer

7. PERFORMING ORGANIZATION NAME(S) AND ADDRESS(ES)

Naval Research Laboratory
Washington, DC 20375-5320

8. PERFORMING ORGANIZATION REPORT NUMBER

NRL/MR/6707--94-7444

9. SPONSORING/MONITORING AGENCY NAME(S) AND ADDRESS(ES)

Office of Naval Research
800 N Quincy Street
Arlington, VA 22217-5660

10. SPONSORING/MONITORING AGENCY REPORT NUMBER

11. SUPPLEMENTARY NOTES

12a. DISTRIBUTION/AVAILABILITY STATEMENT

Approved for public release; distribution unlimited.

12b. DISTRIBUTION CODE

13. ABSTRACT *(Maximum 200 words)*

The development of gyrotrons and free electron lasers over the past decade and a half have naturally led to investigations of additional applications for them. This work looks into applications in the area of atmospheric sensing. Specific gyrotron applications include cloud radars, sensors for atmospheric turbulence, and measurement schemes for upper atmosphere trace impurities. To be useful as atmospehric sensors, free electon lasers must be made much more compact. Several development strategies for accomplishing this are possible. It appears that there are numerous potential applications for both gyrotrons and free electron lasers as atmospheric sensors.

14. SUBJECT TERMS

Gyrotrons
Free electron lasers
Atmospheric sensing

15. NUMBER OF PAGES

69

16. PRICE CODE

17. SECURITY CLASSIFICATION OF REPORT	18. SECURITY CLASSIFICATION OF THIS PAGE	19. SECURITY CLASSIFICATION OF ABSTRACT	20. LIMITATION OF ABSTRACT
UNCLASSIFIED	UNCLASSIFIED	UNCLASSIFIED	UL

NSN 7540-01-280-5500

Standard Form 298 (Rev. 2-89)
Prescribed by ANSI Std 239-18
298-102

CONTENTS

GYROTRONS AND FREE ELECTRON LASERS FOR ATMOSPHERIC SENSING

I. Introduction

Gyrotrons have been developed over the last decade and a half or so for, and to a large extent, by plasma physicists. Free electron lasers (FEL's) were also developed in part by plasma physicists. Gyrotrons have been developed mostly for heating of fusion plasmas, and free electron lasers, as a powerful source of infrared (IR) radiation where none have previously existed. Both of them are generally thought of being situated in large, fixed facilities. In fact, FEL's often *are* the fixed facility, as they require a high energy electron accelerator and a heavily shielded enclosure. However gyrotrons are compact enough that they could be fielded in for instance a small truck. While IRFEL's cannot currently be fielded, there are several possible development strategies which could lead to a fieldable source in the not too distant future.

The field of atmospheric sensing has benefited enormously over recent decades from the use of radar and laser probes. Radars are generally at low frequency, typically X-Band or below, and tunable lasers are usually optical or shorter wavelength. (Fixed frequency or line tunable lasers are available at a few wavelengths in the infrared.) The development of fixed frequency gyrotrons opens up the possibility of cloud radars. Millimeter wave radiation at 94 GHz has the unique capability of scattering weakly from cloud aerosol droplets, which really define the cloud, while at the same time propagating easily through the cloud. It could for instance sense multiple cloud layers, whereas a lidar would be stopped by the first cloud not visibly transparent. Tunable gyrotrons open up new possibilities of absorption measurements over long path lengths. Detection of trace elements at sea level and in the upper atmosphere is also possible. Furthermore, high power gyrotrons, in bistatic radar configurations, open up additional possibilities for remote sensing of clear air turbulence. Tunable, powerful, infrared free electron lasers could allow for the detection of new classes of atmospheric impurities by using them as differential absorption lidars at much greater range.

Manuscript approved January 13, 1994.

II. Gyrotrons, Free Electron Lasers and Atmospheric Propagation

High power gyrotrons and Free Electron Lasers (FEL's) have been developed in the United States and around the world for the last 15 years. In each case, the average radiated power levels now available, respectively in the millimeter wave and infrared regimes, are far in excess of what had been previous capability. At this point, gyrotrons are the most powerful sources of radiation at millimeter wavelength and FEL's have achieved high power in the infrared. While this radiation is generally absorbed in the atmosphere, there are propagation windows. In Fig.(1) is shown the absorbtivity of the atmosphere in the millimeter wavelength[1], and in Fig. (2a) is shown the absorbtivity in the infrared[2]. The white areas correspond to propagation. (These curves are just rough rules of thumb, the actual propagation depends strongly on conditions. Humidity greatly reduces propagation in the millimeter wave regime, and infrared radiation cannot propagate through clouds or fog.) Also shown in Fig.(2b) are the approximate capabilities of various tunable lasers. (Figure 2 was taken partly from Ref. 2, partly from more recent information on OPO's provided by Spectra Physics, and partly from estimates of FEL capability.) Clearly in the infrared region from 3-13μm, free electron lasers constitute a very large breakthrough. In between the millimeter waves and the 13 μm infrared, the atmosphere is for all practical purposes opaque. Naturally to be a useful source for atmospheric sensing, each source would have to be fielded, perhaps on a car or truck, train, ship, aircraft or space craft. Here we briefly review some of the important characteristics of each source and discuss the prospects for fielding it.

1. Gyro Devices at around 94 GHz

Gyrotrons have been developed all over the world[3-11]. As they were developed for heating of fusion plasmas at frequencies ranging from 35-140 GHz, they are inherently long pulse and have high average power capability. In fact, their average power is larger than what is usually required for a radar. Varian gyrotrons[12,13] are available commercially with cw power of 300 kW at 28 GHz, 200 kW at 60 GHz and 100 kW at 140 GHz. The efficiencies of the Varian gyrotrons are all around 30%. A table[14] of several Russian gyrotrons with Gaussian mode outputs, is shown in Table 1. Also commercially available gyrotrons are available in Russia, from the collaboration of the Institute of Applied Physics (IAP) in Nizhny Novgorod and the

Tory Company in Moscow. One available there, which we will mention shortly is the 83 GHz cw gyrotron at a power of 10 kW. A millimeter wave radar with these peak sorts of peak powers, and a duty factor of 0.1-10%, constitutes a breakthrough in millimeter wave radar power by several orders of magnitude. However it is fairly modest as regards gyrotron capability.

One of the few gyrotrons designed at a frequency optimized for atmospheric propagation is the NRL 94 GHz gyrotron[15,16]. This has generated up to 200 kW of power at 94 GHz with efficiencies of about 20%. This frequency is the clearest part of the atmospheric propagation window. Also tunable gyrotrons have been developed at NRL. [11]

The development of powerful gyro amplifiers at frequencies near 94 GHz is also proceeding. For many radar applications, an amplifier is preferable to a free running oscillator. This allows phase and amplitude control of the transmitted beam. If an amplifier and an oscillator are both available, and all other things are equal, the amplifier is the preferred rf source to power a radar. For one thing, data processing is simpler if the amplitude and phase are precisely known pulse to pulse. Nevertheless the data processing can be done with an oscillator transmitter. Also, it may be necessary to coherently combine power from one or more sources. This can only be done with totally coherent signals produced by an amplifier. Counterbalancing the advantages of amplifiers are the fact that they are more complicated and expensive than oscillators, due to the necessity of having the additional microwave plumbing for the input signal. Also there are more stringent requirements of avoiding both oscillation and intercavity cross talk anywhere in the amplifier, which is usually longer than an oscillator. For an atmospheric sensor application, the choice of an oscillator or amplifier will be made in terms of requirements as well as price and availability of whatever the source would be.

At this point the most advanced is a gyroklystron developed at the Institute of Applied Physics (IAP) in Nizhny Novgorod in Russia[17] which has generated power in excess of 50 kW at 94 GHz. The NRL quasi-optical gyrotron, when run in a gyroklystron configuration has also demonstrated capability as both an amplifier and a phase locked oscillator[18,19]. The basic difference is that the IAP gyroklystron uses relatively low Q cavities so that its bandwidth is relatively high, some fraction of a percent. The quasi-optical gyroklystron uses a

much higher Q cavity, so its bandwidth is much less. The two are complementary in that the former could find application where bandwidth is required; the latter where great frequency and phase stability is required.

All gyro devices at 94 GHz use super conducting magnets, although future developments of high harmonic gyrotrons might render these unnecessary[20]. However if one can live with the constraints of a super conducting magnet, any of these gyrotrons are reasonably compact, certainly compact enough to be transported on a small truck or multi-engine aircraft. Thus they could be fielded as radars. We now discuss the sources in somewhat more detail.

A. The NRL 94 GHz Gyrotron

The 94 GHz gyrotron is a TE_{13} mode gyrotron which has generated 150 kW of power in a 1μs pulse at an efficiency of 15-20%. With appropriate cooling on the collector and window, it could operate at an average power of 10 kW. This is in fact only 10% of the average power Varian has demonstrated in their 140 GHz gyrotron. Another advantage to the mode selected is that it can be fairly easily converted to a fundamental TE_{11} mode for propagation. A mode converter has been developed by General Atomics, San Diego, Cal, and is currently in place on our gyrotron. Conversion to the TE_{11} mode has been demonstrated. The measured far field mode pattern of the NRL 94 GHz gyrotron in Fig.(3) shows that the output is in fundamental mode.

Figure 4 is a schematic of the gyrotron with the mode converter in place, Fig 5 is a photograph of the gyrotron laboratory. Figure 2 shows the two stage mode converter ($TE_{13} \rightarrow TE_{12}$ followed by $TE_{21} \rightarrow TE_{11}$). The equipment is compact and can easily be transported on a small truck. This capability to radiate average powers of order 10 KW at 94 GHz into the atmosphere represents a very new capability.

Another important figure of merit for the gyrotron oscillator is bandwidth, which directly translates to range resolution in a radar. Since the Q of the NRL gyrotron is 600, this corresponds to a relatively wide bandwidth. The gyrotron can be tuned by varying the voltage during a pulse. Shown in Fig.(6) is a plot of the

frequency variation of the NRL 94 GHz gyrotron, generated by a time dependent simulation, where the voltage increased from 60 to 70 kV in about 20 nsec (the time chosen for numerical convenience). Here the chirp is about 200 MHz, corresponding to a range resolution of about a meter for optimal data processing in the receiver circuit. Operation of the NRL 94 GHz gyrotron at different voltages have basically confirmed this calculation.

B. The Tunable NRL Quasi-Optical Gyrotron

The quasi-optical gyrotron is a very different sort of a gyrotron in an optical resonator. It has been developed at both NRL[21-24] and Lausanne[25]. The beam propagation and the magnetic field are both transverse to the axis of the resonator. The mode output is taken by diffraction around the mirror. The diffraction is characterized by a fractional loss ν per round trip of the radiation. Typically the NRL experiment runs with ν's between 1 and 5%. In theory and in fact, the resonator operates only in the lowest order fundamental transverse mode.

Figure 7 is a photograph of the quasi-optical gyrotron. It is about as portable as the conventional gyrotron. The maximum power it has achieved so far is 600 kW, but at relatively low 8% efficiency. More recent experiments, at the 100 kW power level have used a number of schemes to increase the efficiency. The maximum efficiency achieved so far is about 20% without a depressed collector and 30% with one[18,19]. While the efficiency of the quasi-optical gyrotron is typically lower than that of a cavity gyrotron, this is largely counterbalanced by the fact that because of its cross bore geometry, a single stage depressed collector is particularly simple to implement.

One of the most attractive features of the quasi-optical gyrotron is its tunability. It can be tuned in three ways: • The magnetic field can be varied over a fairly wide range. The power is relatively insensitive to field. Figure 8a shows a plot of mode frequency and power as a function of magnetic field for a series of lower power experiments. The device can tune over about half an octave from about 80 to 130 GHz. • The device can be tuned with the beam voltage. Since the frequency scales as B/γ, the frequency can be raised by lowering the voltage. Figure 8b shows the Voltage tuning curve. Clearly the power is now sensitive to voltage if only

because the input power is proportional to it. However this voltage dependence does allow rapid tuning over a small frequency range • The cavity can be tuned by adjusting the mirror separation, which can be done without breaking vacuum. This allows for very precise tuning.

It is also possible that the quasi-optical gyrotron could operate at the second harmonic. The Lausanne experiment has already seen evidence of harmonic operation. If it can run with harmonic operation, it opens the possibility of a single source covering the entire spectral region from 80 to 260 GHz.

C. The IAP 94 GHz Gyroklystron

The IAP amplifier development program is the most mature at this point[17]. It has developed powerful tubes at 35 and 94 GHz which have been reported only recently. A 94 GHz gyroklystron has been developed at IAP and is a four cavity interaction circuit. The cavities are all in the TE_{01} mode. Shown in Fig.(9) is a schematic of the interaction circuit superimposed on the background magnetic field. At the peak, the field is 37 kG. In Fig. (10) is shown a plot of its power, gain and bandwidth. In this case the achieved power is 60 kW and the bandwidth is about 400 MHz. For the data shown here, the efficiency was somewhat over 30%. While the IAP program has been in existence for a long time and is quite mature, only recently has information on it been available.

D. The NRL Gyroklystron Amplifier

This configuration uses a Fabre Perot resonator with both the electron beam and magnet field direction perpendicular to the axis of the resonator. Just upstream from the main resonator is a small, lower Q prebunching resonator. At the currents and perpendicular velocities of the beam, this upstream resonator is always below start oscillation threshold[18,19]. The experiment was done at 85 GHz because that was the frequency of the available drive source. It was an extended interaction oscillator (EIO) which put out a power of 1 kW for a 2 μs pulse. Power from the EIO was fed into the upstream resonator, it prebunched the beam, and the amplified power was extracted at the main resonator. A schematic of the quasi-optical gyroklystron is shown in Fig.(11).

Since the main resonator had a very high Q, the bandwidth was very low, about 3 MHz, which is about equal to ω/Q. A plot of amplification as a function of cathode voltage, as compared with a numerical simulation is shown in Fig.(12). In this series of experiments, the power is about 30 kW and the efficiency is about 10%. By increasing the current somewhat, one can exceed the start current in the main cavity, but remain below it in the prebunching cavity. In this case one can drive a phase locked oscillator. Here the oscillator is no longer free running, but has its phase controlled by the much weaker input signal. This is an alternate realization of a phase controlled source. When run as a phase locked oscillator, the device had a power of 60 kW and an efficiency of 16%. In Fig.(13) is shown the phase locking bandwidth as a function of input to output power ratio. The curve is Adler's classic theory[26] for the case of phase locking by direct injection of power into the output port of the device. This is

$$\delta f_L = (f_o/2Q)[P_i/P_o]^{1/2}$$

where δf_L is the locking bandwidth and P_i/P_o is the injection/output power. Clearly the prebunching allows one to greatly exceed the Adler theory. Also because power is injected into a prebunching cavity and not the output, there is no need for a high power millimeter wave circulator.

The quasi-optical gyroklystron is inherently a much narrower band than the conventional cavity configuration. Thus it would find its application where great frequency stability is the most important characteristic. An example might be a radar whose main role is to do Doppler sorting of a large number of low cross section targets with slightly different velocities. Also it does have additional advantages due to its simplicity, intercavity isolation, and adaptability. None of the cavities has any inherent frequency other than c/L_m where L_m is the mirror separation, so it will have a very large inherent tuning range. The cavities are naturally isolated from one another, and at no point during the experiment was there ever any evidence of cross talk. Furthermore, while the cavity Q was very high, this too is flexible and can be lowered by moving the mirrors closer together and by changing the radius of the mirror edge so as to vary the output coupling. Thus the bandwidth and the power can be increased with straightforward scaling.

2 Infrared Free Electron Lasers

Free electron lasers are currently large facilities which take up an entire building, often a very large one. As currently configured, they cannot be fielded. There are two reasons the facilities are so large. First of all, they require a multi megavolt electron beam; and second, because of this beam, they need a tremendous amount of radiation shielding. Thus there are two requirements to field an FEL. First one must reduce the beam energy as much as possible; and second, one must recover as much of the beam energy as possible with the use of a depressed collector. There seem to be two FEL configurations which could potentially evolve toward a device which can be fielded.

The first is the electrostatic accelerator use in the University of California at Santa Barbara (UCSB) FEL[27]. In this device, the beam energy is already recovered with about 90% efficiency in a lasing system, and higher beam recovery can be envisioned with better beam optics. The beam energy in Ref.(27) varies up to 6 MeV. With the magnetostatic wiggler, the wavelength of the radiation varies from about 200μm to 1 mm. Thus, while this experiment recovers the beam energy, it is still too large and it does not operate at the right wavelength. The key to making it smaller is to use a beam energy of 3 MeV. In this case the accelerator is about 16 feet long, 4 feet in diameter and weighs about 4000 pounds, easily small enough to be fielded in a truck, train, ship or even aircraft[28]. Figure 14 is a photograph of a 3 MeV electrostatic accelerator. In order to radiate in the 3-13 μm propagation window, the wiggler wavelength has to be greatly reduced. One way to do this is with the use of an rf wiggler. One particular configuration, using a quasi-optical gyrotron at the second harmonic to form the wiggler, has been analyzed. It was concluded that a portable system, which radiates about 100 Watts of average power in this wavelength regime could be developed[29].

A second possible configuration utilizes a compact FEL such as has been developed at Los Alamos[30]. This employs a 10-15 MeV high gradient rf linac with the beam produced by a photocathode, and a small period microwiggler. It would generate tens of Watts of average power in the 3-13 μm wavelength regime of interest. A schematic of the LASL FEL is shown in Fig. 15. The equipment is all table top size, and if this were the only consideration, it could easily

be fielded. Unfortunately it is not so simple because of the issue of radiation shielding. The Los Alamos system is surrounded by concrete walls four feet thick and is covered by a steel roof six inches thick. However this only shields against the reflected bremstrahlung; the main radiation shield is a below ground beam dump. To field such a device, one would clearly have to collect the beam energy, perhaps with a second rf linac downstream from the FEL and phased so as to collect the beam energy. Los Alamos has attempted this on a larger FEL and has managed to recover about 2/3 of the beam energy in a lasing system[31]. One Stanford FEL also recirculated the beam energy; however this is in a superconducting system which is very large[32]. In any case, if a means can be found to recover the beam energy in the Los Alamos compact IR FEL, this could lead to a fielded system also.

To summarize, gyrotrons already exist in fieldable systems, and there is every reason to believe that IR FEL's can be developed to this point also.

III. Cloud Radar Studies with High Power Gyrotrons

High power millimeter wave sources open the possibility of a variety of active measurements of the atmosphere. The wavelength is one where very few measurements have been done up to now. Millimeter waves have the difficulty that they are absorbed in the atmosphere, either weakly or strongly depending on wavelength and atmospheric conditions, principally humidity as shown in Fig. 1. For very humid conditions at 94 GHz, the loss is about 1 dB/km. This is fairly lossy, but also not so much that high power could not greatly enhance the range. For instance by moving the average power from 4 Watts to 4 kW, the additional propagation distance is increased by 15 km (30 km round trip) in the worst conditions. Furthermore, this loss is only at sea level where there is considerable water vapor in the atmosphere. For propagation at angles to the horizontal, the situation improves quickly. As a rough rule of thumb, the water vapor absorption at 94 GHz is in the lowest 2 or 3 kilometers of the atmosphere.

Millimeter waves have the advantage that they propagate well through particulates, but scatter off them strongly enough to give easily detectable signals, particularly for high power radar transmitters. Conventional radars at microwave frequencies really do not scatter from particulates at all. Lasers radiation, on the other hand, scatters very strongly from particulates, but too strongly. Water clouds for instance are virtually opaque. A laser is basically a line of sight remote sensor. Thus a millimeter wave radar could resolve multiple cloud layers. A low frequency radar would not see them at all, and a laser would see only partially into the lowest layer. In this section, we focus mostly on clouds, because they are very important for meteorology and global warming. However with a sufficiently powerful source, even a clear atmosphere can, and has given rise to detectable return signals at millimeter wavelength.

A. Millimeter Wave Cloud Radars

One of the most promising applications for fixed frequency gyrotrons as atmospheric sensors is cloud radars. These have potential application both as ground and air based systems for the fundamental studies of cloud dynamics. Furthermore, space based 94 GHz radar systems could give real time, world wide maps of the altitudes, thickness and flow fields of clouds. This information is difficult to obtain directly in any other way. Clouds are extremely

important in the earth's albido. It has recently been pointed out that the effect of clouds can dominate by a large factor, the effect of greenhouse gases in global warming[33]. Thus cloud sensors must play an essential role in environmental research.

There are several features of clouds which give rise to radar returns. First there is clear air turbulence in the cloud. This scatters preferentially low frequency radiation, frequencies of 10 GHz and lower. However in scattering from turbulence one is not really sure whether the turbulence is in the cloud or outside of it. Furthermore, it is difficult to directly correlate the turbulence with the cloud physics. Secondly, there are raindrops, ice crystals and snow flakes in the clouds which scatter the radar wave. However the majority of clouds, particularly in their formation stages do have these. Finally, there are the aerosols themselves which define the cloud. These aerosols have very small diameters, typically about 10μm. Since the scattering cross section of the individual aerosol scales as λ^{-4}, where λ is the radar wavelength they can only be observed at millimeter wavelength.

There have already been a number of studies of clouds using 94 GHz radars[34-38]. In Fig.(16) is shown a 94 GHz radar image of a cloud, taken from L'Hermitte's Ref.(36). However these radars all use extended interaction oscillators (EIO's) and are very limited in average power, typically to about 4 Watts. This greatly limits the capability of the system as regards to, minimum reflectivity of the cloud, range in humid air, and the amount of data that can be accumulated in the cloud.

In this section we discuss the use of the gyrotron oscillators or amplifiers for remote sensing of clouds, although any particulate atmospheric pollutants could be sensed by the same principle. Clouds are made up of small water droplets whose diameter ranges from about 10 to 40 μm, and whose droplet density varies from about 0.1-100 aerosols cm^{-3}, depending on the cloud type.

B. Radar Scatter from Clouds

Since the droplet diameter in the cloud is much less than a quarter of the wavelength, the scattering is in the Rayleigh regime and the cross section is given by

$$\sigma = \pi^5 |K^2| D^6/\lambda^4, \qquad (1)$$

where D is the aerosol diameter, λ is the wavelength, and $K = (m^2-1)/(m^2+2)$ and m is the index of refraction. For water at millimeter wavelength, $|K^2|$ is given by about 0.8. The strong increase of cross section with inverse wavelength is a potential advantage of a millimeter wave system. So is the fact that a tightly focused beam can be produced with a relatively small antenna. Since the radar beam intersects the entire cloud, the radar cross section is the cross section of each droplet times the number of droplets in the beam. The volume of the cloud examined is the area of the radar beam times the range resolution distance, denoted h. For cloud studies then, it is the radar reflectance η, the cross section per unit volume, that is the usual parameter used. Here $\eta = n\sigma$ and n is the density of droplets per unit volume. The radar range equation becomes $P_r = P_t h A_e \eta / 4\pi R^2$, where A_e is the effective area of the receiving antenna.

Let us consider the radar return from a single scatterer in the cloud. Say the incident radar pulse is given by

$$E_t(t) = \int df\, G_t(f) \exp 2\pi i f t \equiv e_t(t) \cos[2\pi f_o t + \phi_t(t)]. \qquad (2)$$

Here f_o is assumed to be the carrier frequency and e and ϕ are assumed to vary very slowly in time compared with f_o. Each is assumed to be known and identical from pulse to pulse. The return signal can be constructed as in Section 2. It is

$$e_r(t) \exp i\phi_r(t) = s\, e_t(t-2R/c) \exp\, i\phi_t(t-2R/c)$$

$$\times\ \exp i[-(4\pi i f_o/c)(R+vt)] \qquad (3)$$

where s is proportional to the square root of the cross section, R is the range and v is the droplet velocity. Often the radar signal can be analyzed by forming the matched filter response, defined as

$$M_n = \int dt\, e_t(t-t_n) e_r(t) \exp i[\phi_r(t) - \phi_t(t-t_n)] \equiv$$

$$\int dt\, s e_t(t-t_n)\, e_t(t_i) \exp i[\phi_t(t_i) - \phi_t(t-t_n) - 4\pi f_0 R_i/c]. \qquad (4)$$

That is the matched filter response is the convolution of the time reversed transmitted signal delayed by time t_n with the received signal. The matched filter has two very desirable properties, one

that it maximizes the signal to noise power, and second that it is a simple way of converting the bandwidth of the transmitted pulse into range resolution[39].

Consider the case of a Gaussian pulse with linear frequency chirp. If we take $e(t) = e_0 \exp-[t/T]^2$ and $\phi(t) = 0.5\alpha t^2$, then we find for the matched filter response

$$M_{ng} = (\sqrt{\pi}/2)e_0^2 T \exp(4\pi i f_0 R/c)$$

$$\times \quad \exp\{-(t_n - 2R/c)^2[1/2T^2 + \alpha^2 T^2/8]\}. \qquad (5)$$

The range resolution is determined by the fall off of the Gaussian. If this is dominated by the frequency chirp, the range resolution goes roughly as $c\alpha T/\sqrt{8} \approx c/\Delta f$ where Δf is the frequency spread of the transmitted pulse. Note that the matched filter response falls off very quickly with range, so targets can be separated in range even if large and small targets are much nearer to each other than cT.

If an oscillator is used instead of an amplifier, there is no guarantee that the transmitted waveform will be identical from pulse to pulse. However one can still renormalize the transmitted pulse to a desired transmitted pulse, for each pulse in the pulse train, and do effectively the same thing. This was discussed in detail in Ref.(40), which introduced the notion of a *desired pulse*, which the actual pulse is normalized to. While one can use an oscillator and renormalize for each pulse, the price to pay is that much more data processing is necessary and also that bandwidth is not used as effectively.

C. Analysis of Radar Returns from Clouds

Here we briefly examine the use of a gyrotron oscillator or amplifier as a transmitter for radar studies of clouds. We base the processing scheme on the matched filter response, as just discussed. The cloud consists of a number of individual scatterers denoted by the index i. Each scatterer moves with velocity $v+\delta v_i$, where v is the average velocity in the range cell and δv_i is a random velocity whose average value is zero. Each velocity is sufficiently small that the

scatterers can be regarded as stationary during the individual radar pulse. However the velocities will be Doppler resolved by looking at reflections from a long sequence of pulses. The return signal can be constructed by summing over the returns from the individual scatterers. It is

$$e_r(t)\exp i\phi_r(t) = \Sigma_i\, s_i\, e_t(t-2R_i/c)\exp\ i\phi_t(t-2R_i/c)$$

$$\times\quad \exp i[-(4\pi i f_o/c)(R_i + vt + \delta v_i t)] \qquad (6)$$

There is not a single transmitted pulse, but a large number of pulses separated by interpulse time τ. Let p be the index denoting pulse number and P be the total number of pulses in the pulse train. We now calculate the matched filter response for the p^{th} pulse for the n^{th} range interval. Assuming that the pulse, in the case of an amplifier, or the *desired pulse* , in the case of an oscillator, is Gaussian, the matched filter response is

$$M_{np} = (\sqrt{\pi}/2)e_0^2 T\Sigma_i s_i \exp-[(4\pi i f_o/c)(R_i+(v+\delta v_i)p\tau)] \qquad (7)$$

where the index n denotes the range cell and p the pulse. We assumed each droplet is at the center of the range cell, and the summation is over the droplets in the range cell. Associated with the index p is the Fourrier transform variable $2\pi z/P$ where z takes on integer values from zero to P-1. Then one can define

$$Q_n(z) = \Sigma_p M_{np}\exp 2\pi i p z/P \qquad (8)$$

To obtain the reflectance, one forms the summation $\Sigma_z|Q_n(z)|^2 \equiv Q_n$. In addition to the summation over z, there are four other summations over i and p and over the analogous variables j and q in the complex conjugate summations. The summation over z is a simple summation of a geometric series and turns out to be equal to P if p=q and zero otherwise. We then separate the summation over i and j into a sum of two summations, one having i=j and one having $i\neq j$. The former is a simple summation over reflectance's over the individual droplets and has N terms in it where N is the number of droplets. The latter is the sum of 0.5N(N-1) terms, each one having a random phase assuming the droplets are uncorrelated. Thus the ensemble average of this summation is zero. The problem is that any single pulse return is not an ensemble. The rms value of a summation of N^2 random phases is about N, so for each value of p,

the summation over the i's and j's will have about the same order of magnitude. For the case of a sequence of pulse returns, we can often exploit this summation over the sequence to give the ensemble average. (In classical statistical mechanics, the time average and ensemble average are assumed to be the same.) In this case, the summation over the p index greatly reduces the value of the $i \neq j$ summation. In this summation, the sum over p is also a geometric sum which can be done simply. The result is that this summation is very small unless $\delta v_i - \delta v_j < c/4f_0 P\tau$. Thus if the velocity spread of the droplets is sufficiently large, the $i \neq j$ sum is small compared to the $i=j$ sum. If f_0 is 94 GHz, and $P\tau = 0.1$ sec, the spread of droplet velocities only has to be large compared to 1 cm/s, a condition almost certainly satisfied for droplets in clouds. Thus we find that

$$Q_n = \{0.8P^2\pi^7 e_0^4 T^2 d^4 \exp(-2\alpha R_n)/16\lambda^6 R_n^4\} \Sigma_i D_i^6 \qquad (9)$$

where we have used the relation between s and σ for the droplets, the expression for cross section in Eq.(1), and the fact that the antenna gain is $\pi^2 d^2/\lambda^2$, where d is the antenna diameter.

To determine the average velocity of the droplets, one forms the summation $\Sigma_z z|Q_n(z)|^2 \equiv F_n$. An analogous calculation gives the result

$$F_n = [2Pf_0 v_n \tau/c] \times Q_n \qquad (10)$$

where we have explicitly denoted the dependence of velocity on range cell. Other moments of the distribution of velocities can be found by taking other moments of Q_n. Equations (9) and (10) show how the reflectance and relative velocity in a range cell are calculated from the backscattered radar signal.

D. High Power Millimeter Wave Atmospheric Probes

We will briefly review some of L'Hermitte's studies[34-37] of clouds using a low power source, and then discuss ways in which the system could be enhanced at higher power. Then we discuss briefly some initial results on high power millimeter wave probing of the clean atmosphere.

L'Hermitte studied, among other things, small cumulus clouds and intense thunderstorms, both around Miami, Florida. He does not use an amplifier as his microwave source, but uses an oscillator. To do the coherent signal integration and Doppler processing, he uses a coherent on receive approach and corrects the phase of the received signal according to the phase of the transmitted signal[41]. Except for the random phase from pulse to pulse, the EIO has extremely good signal properties. In fact, this was the reason for Lhermitte's choice of an EIO over a magnetron, which could operate at somewhat higher average power.

For a typical cumulus cloud, like those studied by L'Hermitte, the droplet diameter is about 10μm and the droplet density is about 100cm^{-3}, so the reflectivity is about 3×10^{-12} cm^{-1}. With such small reflectance's and low power of the transmitter, the observation of the cloud is difficult. For Lhermitte's case, with a range of 2 km, a transmitted power of 1 kW, a range resolution distance h of 6×10^{3} cm, and an effective aperture of 4×10^{3} cm^{2}, the received power is about 10^{-13} W. The noise power of an ideal receiver at 300°K is about 10^{-14}W if the bandwidth is pulse length limited to 2×10^{6} s^{-1}. However Lhermitte's receiver has an actual noise of about 5×10^{-13}. His signal power is below the noise power, and he had to integrate the signal over a considerable number of pulses to get good data. In his case, he runs the EIO at about 10 kHz pulse repetition rate and integrates for 3 s, or about 3×10^{4} pulses. He finds that the meteorological conditions remain reasonably constant for these 3s.

One of L'Hermitte's other observations was the reflection of the radar wave from a thunderstorm in the Miami, Florida area. The range at which he was able to operate was about 20-30 km. However since the air at ground level was quite humid, he was only able to observe the tops of the clouds. For instance one of his observations is at an angle of 34° and a range of 20 km, so that he observes an altitude of 11 km. He points out that at a 30° elevation, the two way absorption was 12 dB, whereas at a 7° angle, it is 50dB.

Now let us discuss the way these cloud measurements could be enhanced at higher transmitted power. For the case of the thunderstorm, the additional power could be directly used to overcome absorption in the humid air. For instance a 4 kW average power system would overcome an additional 30 dB of atmospheric absorption and allow observation much lower in the thunderstorm.

Now consider the observation of the cumulus cloud. A small cloud passes directly overhead at an altitude of about 1.5 km; as it goes by, the reflectivity and vertical velocities are measured by the radar at a series of range cells 65 m in depth. The cloud is overhead for about 2 minutes. Since each vertical scan takes 3 s, there are about 40 vertical scans in the cloud and about 6-8 range cells. A higher power transmitter could enhance these measurements in a number of ways. First, in doing the same measurement as L'Hermitte at higher power, the radar beam could be scanned from side to side in the cloud so that a three dimensional image of the cloud could be formed. Second, the range cell could be reduced to perhaps 10 m (a 10 MHz bandwidth) so that the cloud could be examined vertically in much greater detail. Third, the higher power could be used for greater range to image clouds that are not directly overhead. This not only gives another view of the cloud, but it also gives another component of velocity. For clouds with a horizontal range of perhaps 10 km, the radar would give a Doppler velocity in a direction that is almost horizontal.

The other very important application for 94 GHz cloud radar studies is the proposed space based radar. Here the power required is greater than the 4 Watt system used up to now. Finally David Atlas[42,43] has recently pointed out a number of fundamental issues with regard to cloud dynamics that can be effectively studied with 94 GHz radars. Some of these issues are enumerated in Table 2.

We conclude by discussing a recent experiment on probing the clear atmosphere with a high power 84 GHz gyrotron[44]. The experiment was cw and the transmitter had a power of 10 kW. The receiver had a sensitivity of 5×10^{-14} W, and the returned signal was enhanced by using a 10 second integration time. The transmitted beam was scanned in angle, and at certain angles, there were strong backscattered signals. It is most likely that these signals are the result of particulates, probably at the top of the atmospheric inversion layer, at 100-300 meters altitude. Clear air turbulence was a possible scatterer, but if so, the turbulence would have had to be extremely intense to give rise to scatter at such small wavelength. Additional experiments are planned in the future to further investigate these phenomena.

IV. Remote Sensing of Atmospheric Turbulence

Here we discuss the potential use of the quasi-optical gyrotron as a remote sensor for atmospheric turbulence. High power gyrotrons appear to provide a unique capability for sensing the inner scale length of the turbulence in an open atmosphere at fairly long range. This is an important property, because standard theories relate it closely to the strength of the turbulence. Before proceeding, we briefly review some properties of atmospheric turbulence as summarized in Doviak and Zrnic[45].

Power feeding the turbulence is provided at large scale length. Nonlinear convection of the fluid then generates shorter and shorter scale lengths until the very short scale motions are dissipated by viscosity. This intermediate range of cascade is called the inertial range. The energy per unit mass of the fluid per unit k is dE(k)/dk and has units m^3/s^2. The power per unit mass provided at small k is denoted ε, and it has units m^2/s^3. For steady state turbulence, ε is also the power dissipated per unit mass at large k, which is also equal to the power convected through the inertial range in k space. The convection velocity through k space, dk/dt, is related to E and ε through the relation $\varepsilon = (dk/dt)\times(dE(k)/dk)$. The assumption now is that E(k) depends only on k and ε. Assuming a polynomial relation, there is only one which is dimensionally correct,

$$dE(k)/dk = A\ \varepsilon^{2/3}k^{-5/3}, \qquad (11)$$

where A is a dimensionless constant. Doviak and Zrnic use the value of ε to characterize the turbulence, Table 3 gives their characterization. Generally, the spectrum seems to be borne out by experiment.

The minimum value of k is determined by the power input at large scale. The maximum value of k is determined by the viscous dissipation. The time for the power in this range of k to dissipate by viscosity is given by $1/\nu k^2$, where ν is the kinematic viscosity in m^2/s. The time the spectral energy remains in a region of size k is given by k/(dk/dt). Equating these two times, we find that k_{max} is proportional to $\varepsilon^{1/4}/\nu^{3/4}$. Doviak and Zrnic give the proportionality of 1/5, so

$$k_{max} = 0.2\varepsilon^{1/4}/\nu^{3/4}. \qquad (12)$$

At sea level, $\nu \approx 10^{-5}$ m^2/s, so for strong turbulence, the minimum distance, $2\pi/k$ is about 1 cm.

Scattering from clear air turbulence is caused by fluctuations in the index of refraction which in turn is caused mostly by fluctuations in water vapor content. To determine the spectrum of index of refraction fluctuations, the spectrum of a scalar quantity passively advected by the turbulent field must be calculated[45-47]. The basic assumption of all workers, however, is that the passively advected scalar has the same spectrum as the energy, so $|n(k)|^2 = C_n^2\, k^{-5/3}$, where C_n^2 is in units of $m^{-2/3}$. Doviak and Zrnik's characterization the coefficient C_n^2 in terms of the strength of the turbulence is also shown in Table 3.

We now consider the scattering from the turbulence. Assuming that δn is small, the Born approximation for the case that the electric field is evaluated in the far field ($k_o D^2/r<1$, where D is the diameter of the scattering volume), gives the scattered electric field at the point r is given by

$$E_s = (k_o^2 E_i/4\pi r)\exp ik_o r \int d^3r' \delta n(r') \exp\, i(k_i - k_s)\cdot r' \qquad (13)$$

where E_i is the incident electric field in the scattering region, k_i is the incident, and k_s is the scattered wave vector. The integral is over the scattering volume, which is defined as the intersection of the patterns of the transmitting and receiving antennae. Assuming that the scattering volume is very large compared to the scale size of the index fluctuation, we find

$$|E_s|^2 = k_o^4 E_i^2 V C_n^2 |k_i - k_s|^{-11/3}/8r^2 \qquad (14)$$

where V is the scattering volume. In performing the integrals and manipulations, we have made use of the fact that the spectral density per unit k space volume is given by $|n(k)|^2/4\pi k^2$ for a homogeneous, isotropic spectrum. Also, we have made use of the fact that the density of states in k space is $V/(2\pi)^3$. If the scattering angle is θ, then $|k_i - k_s| = 2k_i \sin\theta/2$.

For backscatter ($\theta=\pi$) and $k=1800 m^{-1}$ (94 GHz), the scattering wave vector is almost certainly larger than k_{max}, so there should be virtually no backscatter. However there will be scatter in other

directions. The use of powerful gyrotrons at 94 GHz (and possibly at 35 GHz also) opens up the possibility of examining the inner scale length by oblique scattering measurements. The inner scale length could be inferred from the angle at which the scattering disappears.

Let us consider a specific example to show how the availability of 94 GHz gyrotrons with over 100 kW of power can render possible a scattering measurement of the inner scale length. The scattering volume is then roughly LD^2 where L is the length of the intersection of the two antenna patterns and we have assumed the incident beam is the more tightly focused of the two. Then we relate the field amplitude to the power density and add to Eq.(14) additional factors accounting for the atmospheric attenuation. Then Eq.(14) can be rewritten as

$$P_r = k_o^4 A_e L P_t C_n^2 |k_i - k_s|^{-11/3} \exp[-\alpha(r_i + r_s)]/8r_s^2 \qquad (15)$$

where $P_{r(t)}$ is the incident (reflected) power, A_e is the aperture of the receiving antenna, α is the atmospheric attenuation, and r_i is the range from the incident antenna to the scattering region. Let us choose a configuration in which the scattered radiation is in the far field. Although this is not absolutely necessary, it does simplify both the analysis and the interpretation of any data.

Take a transmitting antenna of D=3 m which can focus radiation down to a spot 2 m, 2.5 km away, and a range to the receiver of 10 km. For relative humidity 50% or less, the attenuation is 10 dB or less. For 94 GHz radiation with a 3 m receiving antenna and an assumed inner scale length of 3 cm ($|k_i - k_s|$=200), we find that $P_r/P_i \approx 2\times10^{-17}$, assuming strong turbulence, $C_n=3\times10^{-13}$, and also $L=D/\sin\theta$. If the incident power is 10^5 W, the received power is about 2×10^{-12} W, 4 times the noise power at 300°K. Integration over a small number of pulses could further enhance SNR. Consider the alternative of using an EIO having a power of 1 kW and an average power of 4 W. Now the signal is a factor of 25 below the noise level, and this is for fairly strong turbulence. It is unlikely that the SNR could be significantly increased by integrating over a large number of pulses; at the shortest scale length (3 cm), the correlation time of the turbulence is undoubtedly very short (10^{-2}s at 3m/s), so the scattered pulses would not be coherent with one another for very long.

A configuration for bistatic remote sensing of clear air turbulence is shown in Fig. 17. A transmitter is on the ground a distance D from the receiver. It points upward at a shallow angle ϕ. The receiver also focuses to a point at which it intersects the transmitted beam at an altitude h. By varying the direction of the transmitted beam, the angle θ between the transmitted and received beam varies, and the scattering can be determined as a function of this angle.

V. Remote Sensing of Trace Impurities in the Upper Atmosphere

We now look into whether the tunability of the quasi-optical gyrotron can be used to detect trace elements. At sea level, this appears to be an extremely difficult measurement due to the fact that the pressure broadening of the absorption lines is substantial (typically about 2-3 GHz), and the impurity concentration is very low. That is the absorption rate at the line center scales as the number density of the impurity in question N_i divided by the collision rate, which is in turn proportional to the ambient density N_a; so that the absorption rate is proportional to N_i/N_a. At sea level, N_a is very large, so the absorption rate is correspondingly small. Distinguishing the impurity absorption from the water vapor absorption, which dominates it by many orders of magnitude, does not appear to be a simple task. However for impurities in the upper atmosphere, the pressure broadening is much less, so N_i/N_a is much greater. Also there is much less water vapor at high altitude to interfere with the measurement.

The idea is then to use a high power tunable source to do an absorption (and possibly also phase shift) measurement as a function of frequency near the absorption line. (One might think that at high altitude, the molecule would spontaneously re-emit before it is collisionally de-excited. However the time for spontaneous re-emission for rotationally excited molecules varies from about 10^4 to 10^9 s, so this is not the case[48].) Measurements like this are currently performed by radiometry, either ground or space based, whereby the thermal spectrum of the atmosphere is measured and related to the trace elements. An alternate scheme is to use a millimeter wave source at high power to selectively (as a function of frequency) heat the upper for diagnostic purposes.

A. Trace Element Determination by Radiometry

In radiometry, the thermal spectrum of millimeter wave radiation is detected and related to the concentration of the element.[48] These measurements can be absorption measurements, for instance measuring the absorption of sunlight at frequencies near the absorption line. Also the thermal emission can be studied, and this is what we concentrate on here. For the atmosphere which radiates as a black body (if it were optically thick) the radiation temperature is related to the intensity of radiation by the Rayleigh-Jeans, or actually the Planck law. If the radiation is emitted from a

region with temperature T and s is the path length, then the radiation temperature T_R at the receiving antenna is given by

$$T_R = \int_h^{\infty} T(s)\alpha(s)\exp-\tau(s), \quad \tau(s) = \int_h^{s}\alpha(s')ds' \qquad (16)$$

where $\alpha(s)$ is the sum of the absorption coefficient of all gases to be considered and τ is the opacity. For a propagation medium which is optically thin, as is the case for millimeter waves in the upper atmosphere, the presence of the gas of interest gives rise to a slight increase in radiation temperature at the frequencies near the absorption line.

The upper atmosphere is typically at a temperature of between about 200-300°K. Thus for an optically thin propagation medium, the ratio of antenna temperature due to the impurity to the source temperature (that is the upper atmosphere) is roughly the opacity. Ozone is a particularly attractive element to detect at millimeter wavelength[49,50]. Fig. 18, from Waters, shows the zenith opacity of the atmosphere as a function of frequency, with the absorption lines of ozone shown. Clearly, there are many possible lines to operate in the millimeter wave band. For ozone at 110.8 GHz, in a standard atmosphere, the zenith opacity is about 6%, so the antenna temperature due to ozone, at this frequency, is about 10° K at the line center. If the line shape is Lorentzian, as is characteristic of a pressure broadened line, the temperature as a function of frequency reflects this line shape. The line width is a function of altitude. If sufficient resolution of temperature as a function of frequency is available, the profile of ozone density as a function of altitude can often be inverted.[51]

This temperature due to the impurity is generally small compared to the atmosphere temperature. In radiometry, the relative temperature fluctuation through a channel of bandwidth B is given by $(BY)^{-1/2}$ where Y is the integration time, so small temperature changes due to an impurity can be resolved by long integration time. Parrish et al[52] have recently studied trace element concentrations in the upper atmosphere. These are all related to the ozone cycle, and as such, the altitudes are about 40 km, so the pressure broadening is about 10-20 MHz. They found that at 277 GHz, ozone had a temperature of 8°K and the integration time was an hour to achieve SNR of 600. They also found that ClO had a temperature about 0.06° at 279 GHz. To achieve SNR of 25 took 36 hours over 9 days. The weakest line they were able to detect was

the 266 GHz line of HO_2. This line had a temperature of about 0.015°K and took 55 hours to resolve the line. Shown in Fig 19a is the result for ozone, and in Fig 19b is the result for ClO from Parrish et al.

Space based millimeter wave radiometry has demonstrated the capability of measuring simultaneously the ozone and ClO profile, world wide in real time. Waters[53] has presented beautiful images of ClO masses moving around the world and devouring ozone. The real time images in Ref 23 change on a time scale faster than the time required for Parrish's measurement. Thus space based passive millimeter wave radiometry appears to be the only way to get the time resolution over the time scales of interest. However these measurements are themselves limited in some ways also. To get a world wide picture of the ozone concentration requires an average over altitude, and to get a dependence on altitude requires an average over a large portion of the earth's surface taken over many orbits. Also the radiometers on the space craft are set at 4 frequencies, so that the trace impurities to be studied are set at the outset and cannot easily be varied, at least those used in Ref. (53). Shown in Fig. (20) are horizontal images of ClO taken over 9 days, taken from Waters et al. Figure 21 shows average vertical profiles of ClO from Ref. 53, where the data is averaged over space and time.

We now discuss the potential use of a tunable quasi-optical gyrotron to do an active measurement of upper atmosphere trace element impurities. There appear to be two basic types of measurements one can do, incoherent or coherent. In the former, the phase information is somewhere lost on the radiation path, and in the former it is not. Finally there is the possibility of using the quasi-optical gyrotron at high average power for selective heating of the upper atmosphere due to power absorption on a particular molecular rotation line.

B. Trace Element Detection by Incoherent Scatter

We now consider the use of a high power tunable source for measurements requiring one or two way transmission and detection of radiation at a set of frequencies near the absorption line. The most natural two way transmission path is reflection from the moon, which is visible from any point on earth about half the time. We specifically envision the use of a quasi-optical gyrotron, with tunability from 80-260 GHz. The radiation will be transmitted from

a ground station on earth and received in a large number of receivers.

The moon subtends an angle of about 10^{-2} radians as seen from the earth. We would like to focus the radiation on as small as possible a spot on the moon, so that the range variation to the target, and thereby the temporal spreading of the reflected pulse is minimized. At 150 GHz, a 2 meter dish can focus the radiation to about 10% of the moon's diameter; a 20 meter diameter millimeter wave qualified satellite tracker can focus the radiation to about 1% of the moon's diameter. Let us assume that the radiation is reflected diffusely from the surface of the moon into a solid angle of about π radians. Take for the radiated power, 300kW and the pulse length, 10 μs. Since the range is about $4x10^8$ meters, the received power in a 2 meter dish is about $4x10^{-13}$ W assuming 10 dB attenuation on the two way path. If the noise temperature of the receiver is about 10^3 degrees Kelvin and its bandwidth is about 10^5 s^{-1}, the signal to noise ratio on a single pulse is about 400.

Thus the signal is quite a bit above the noise. However the moon is a rough surface. That is the surface scattered radiation is described by for instance Eq.(6), where the s_i is now a scattering element on the surface. The problem is that as the frequency changes from say the center to the wings of the absorption line, these scattering elements change phase in an essentially random manner due to the fact that as the frequency varies through the absorption line (at least a few tens of MHz), the phase of the scatterers are randomized. Thus in any two measurements, there are order unity variations between the two received signals if the measurements are uncorrelated. The way to resolve the absorption line then is to do an ensemble of measurements. If each measurement is uncorrelated with every other one, the relative error for N measurements is roughly $N^{-1/2}$. To decorrelate the measurements, one would use different reflection points on the moon. (If the measurements are partially correlated with one another, the fall off in relative error with N is slower than $N^{-1/2}$)[54]. For uncorrelated events, the statistical properties are basically the same as for radiometry; this scheme might be considered radiometry at large signal strength.

Thus for the case of ozone, where the two way zenith opacity is about 12% at 110.8 GHz, roughly 10^4 pulses would be required to give signal to noise ratio of 10 from the center to wing of the

absorption line. For a single frequency, this would take about a second. To resolve the line into ten frequency bands would take about 10 seconds. For the case of ClO, the two way opacity at 278.63 GHz is about 6×10^{-4}, assuming an ambient temperature of 200°K. In order to get a signal to noise ratio of 10^{-4}, about 10^8 shots are needed. If the rep rate is 10^4, f = 278.63 GHz, and the parameters are otherwise as above, then about 3 hours are needed for each frequency on the line. The times here are roughly the same as for passive radiometry, but a much less sensitive receiver is needed.

Now consider the receivers on the ground. To achieve world wide coverage, there would have to be one transmitter, most likely on a mountain top so as to reduce the water absorption of the transmitted radiation on the way up, and a large number of receivers on the ground. Wherever possible the receivers would be placed at as high an altitude as possible, and receivers could even be air based for certain measurements. Since the quasi-optical gyrotron is tunable from about 80-260 GHz, a large number of different impurities could be measured simply by tuning the source. Thus the recent availability of powerful millimeter wave sources open the possibility of ground based, simultaneous, world wide measurements of upper atmosphere impurities. This is illustrated in Fig. 22a.

C. Trace Element Detection by Coherent Absorption Measurements

We now consider coherent scattering. This can be accomplished first by one way propagation, that is the tunable millimeter wave source on a satellite and the receivers on the ground, or vice versa. Alternatively it can be accomplished by two way propagation. Here, millimeter waves are reflected from a satellite, and the absorption and phase shift as a function of frequency across the absorption line provides information regarding the trace elements in question.

We now consider the use of the quasi-optical gyrotron as a tunable source for active detection of ozone. We consider the 110.8 GHz absorption line; a frequency at which the quasi-optical gyrotron can easily be tuned. To provide a two way path, we exploit reflection from an existing satellite. There are many satellites and pieces of space debris whose low earth orbits are known to high precision. As we will see however, not all are suitable as reflectors; to be a viable reflector, the size of the satellite must be quite small.

In active probing of the upper atmosphere, both amplitude and phase are available to analyze. Here we consider only the phase, since the analysis of the amplitude is no different in principle from radiometry. For a Lorentzian line shape centered at ω_o, the total complex attenuation and phase shift, Ξ for the two way propagation is given by

$$\Xi = \tau\nu\{(\nu + i(\omega-\omega_o))/(\nu^2 + (\omega-\omega_0)^2)\}, \qquad (17)$$

where τ/ν is the two way opacity at the line center, and ν is the pressure broadening. At the altitude in question, $\nu/2\pi$ is about 10 MHz. Thus, for ozone, whose two way zenith opacity is 12%, and whose opacity at 45° is about 20%, the total phase shift as one crosses the line could be as high as 10°-15°. If the incident wave is at frequency f_i the phase of the returned signal is given by

$$\phi_{ri}= 2\pi R(2f_i+\delta f_{di})/c + \phi_{ti}(t-2R/c) + \Delta\Phi_i(f_i)$$

$$+ \Delta\Phi_i(f_i+\delta f_{di}) +\Phi +\delta\Phi(f_i,p) \qquad (18)$$

For a satellite of known orbit, the Doppler shift can be calculated very accurately, and can be as high as a few MHz for 100 GHz incident radiation. In Eq.(18), $\Delta\Phi_i(f_i)$ is the ozone generated phase shift at frequency f_i on the way up, $\Delta\Phi_i(f_i+\delta f_{di})$ is the ozone generated phase shift of the Doppler shifted wave on the way down, Φ is the phase shift from all other components, determined from for instance a standard atmosphere model and is assumed to vary only slightly across the absorption line, and $\delta\Phi(f_i,p)$ is the phase shift generated by the satellite, where p denotes pulse number. The satellite generated phase shift varies with frequency because different frequencies have different scattering centers; it varies with p because the satellite might change its orientation, due to rotation, during the pulse train. The difficulty is that $\delta\Phi(f_i,p)$ is basically unknown. One can only perform the measurement if $\delta\Phi(f_i,p)$ is independent of both f_i and p.

The satellite will be considered to be a set of discrete scatterers, with index m, centered at R and having position δR_m from the center. It is the δR_m's which contribute the essentially random nature of the phase. If the frequency difference between the waves

in the spectrum is denoted δf, then the contribution to the phase shift is $4\pi\delta R\delta f/c$, where for convenience, we have deleted subscripts. As long as this is small compared to the phase shift we are attempting to measure, it can be neglected. This then puts a limit on both the size of the satellite and also on the frequency spread. For ozone at 40 km altitude, assume a width of 20 MHz. At a 45^o inclination angle, the phase shift we are measuring is about 0.2 radians. This means that the satellite or debris radius must be small compared to about 30 cm. Also, the phase might change pulse to pulse because of the rotation of the satellite, so the total measurement time must be small compared to a rotation period of the satellite, typically tens of seconds. Thus, a small existing satellite or piece of space debris, which is not rotating violently, could serve as a reflector for rapid, ground based ozone measurement.

We now consider what it would take to do an ozone measurement at a satellite tracker. If we consider the antenna to be 20 m (a gain of 87 dB), a bandwidth which is pulse time limited (10^5 s^{-1}), a transmitted power of 1 MW, a range of 300 km, a 5 cm radius spherical scatterer, and a receiver temperature of 1000^oK, we find that SNR is in excess of 10^6. This corresponds to a phase resolution in a single pulse of about $(SNR)^{-1/2}$. If 20 pulses within a time of a tenth of a second to a second are transmitted within the 20 MHz interrogation bandwidth, the phase shift within the absorption line can be resolved and the ozone density can be inferred.

We now consider a method of making the measurement much more accurate. The satellite generated phase shift can be greatly reduced or eliminated by the use of a specially designed satellite. Specifically, we consider the use of a spherical satellite, whose cross section is independent of orientation, and whose cross section as a function of frequency can be accurately calculated and measured. For trace elements such as ClO or HO_2, discussed in Ref. 52, the total phase shift across the absorption line is 10^{-3}-10^{-4} radians. Thus the satellite must be smooth to about this fraction of a wavelength. However since we are considering millimeter waves, this fraction of a wavelength means an optical quality reflector, a standard capability. We consider specifically a 20 cm radius spherical reflector. In one rocket launch, a number of these, perhaps ten or so, could be placed into orbit to provide nearly continual, permanent coverage. A network of satellite trackers around the earth would then be able to

provide nearly continuous, world wide coverage of any element with an absorption line in the millimeter wave band.

It is interesting to note that the manufacture of metal spheres with this accuracy and launching them into orbit is an established technique. Such metal spheres are made by for instance the Salem Specialty Ball Corporation in West Simsbury, Connecticut[55]. They have been launched into low earth orbit as calibration targets for measuring radar cross section of space debris in the *Orbit Debris Radar Calibrated Sphere* project[56] in 1992 and 1993. (The micron tolerances in radius are required so that they can be shot into space from a shuttle based explosive launcher.) The cost of launching these balls into a sufficiently high earth orbit is not that great, as costs of space flights go. Launching them would cost in the neighborhood of one million dollars.

We now consider reflection from one of these specially designed satellites to measure trace impurity density. For instance the 242 GHz ClO absorption[52] line would be observable with the quasi-optical gyrotron at the second harmonic. It has a limb temperature of few degrees Kelvin, and a ground temperature of about 0.05°K looking near the horizontal. Since an active measurement has double the path length, we assume that at an angle of 45° to the zenith, a value of about 0.03°K, or a phase shift of about 3×10^{-4} radians. The total two way absorption, from sea level, at 240 GHz, at an inclination of 45° to the zenith is less than 10 dB for relative humidity less than 50%. If a high altitude is chosen for the measurement, the absorption is less still. We consider first the use of a satellite tracking station, with an antenna diameter of 20 m. Consider a receiver temperature now of 100°K, a total atmospheric attenuation of 10 dB, and a radiated power, assumed to be 300 kW at the second harmonic. Then for a 10 μs pulse, SNR is about 6×10^{7} . Ten pulses will then give sufficient SNR to accurately measure a phase shift 10^{-4} radians. To conclude, the tunability of the quasi-optical gyrotron gives a capability to rapidly measure upper atmosphere ozone concentrations with existing equipment. With specially designed satellites and accurate satellite tracking, it could give rapid measurement of trace impurities at much lower concentration. A schematic of the measurement technique is shown in Fig.(22b).

For what might be considered the ultimate of such a system, one could place the quasi-optical gyrotron in a high earth orbit

satellite, so that the radiation is focused on the entire visible hemisphere. This would enormously increase the signal to noise ratio since now there is a one way path. The frequency could be tuned to that of the absorber of interest and the signal could be received at a network of ground receiver stations. For instance if the instantaneous radiated power is 100 kW, the received power through a 2 meter dish is about 10^{-8}W, at least 6 orders of magnitude above the noise level for a 300°K receiver with megahertz bandwidth. If the duty cycle of the source is 10^{-3}, and the efficiency is 30%, as has already been demonstrated, the prime power needed for this function on the satellite is only 300 W, assuming that it is radiating all the time. While the cost of launching a high power millimeter wave source into geosynchronous, or other high earth orbit is great, it would provide a tremendous capability for rapid, altitude resolved (by the absorption line profile), worldwide monitoring virtually any upper atmospheric impurity of interest. A schematic of this scheme is shown in Fig.(22c).

Atmospheric Modification With High Power Millimeter Waves

We now consider millimeter wave sources at the very highest achievable average power, the several hundred kilowatt to megawatt level, and examine the possibility of atmospheric modification. We consider here the heating of the atmosphere by the absorption (actually the differential absorption) of this radiated power by the absorption line of interest. Let us consider for instance the 278 GHz line of ClO, for which the opacity as measured by Parrish was about 3×10^{-4}. Let us imagine an average radiated power of 300 kW, so that the absorbed power by the ClO would be about 100 Watts. If this is radiated by a 20 meter, millimeter wave qualified dish, and the ClO which does the absorption is spread out between about 30 and 40 km, this then gives an additional heating rate in the radiation beam of about 10^{-5} degrees Kelvin per second. If the loss is due to thermal conduction to the cooler gas outside of the beam, the temperature rise of the gas in the beam would be limited to about 2°K. As we have seen, this temperature raise can be measured by conventional radiometry along the boresight. For ozone, a 110.8 GHz, the power required to measurably heat the atmosphere are very much less. Thus by using the tunable millimeter wave source, at its highest average power to heat the atmosphere, one can detect elements with as low a density as that of ClO.

VI. Atmospheric Sensing With Free Electron Lasers

The field of remote sensing of the atmosphere with lasers is an enormous[2,57] one and we will only give a very brief discussion here. As is apparent in Fig. (2), FEL's, if they could be portable and fielded, could give a breakthrough capability in the infrared for the case that tunability is required. Tunability is required mostly for differential absorption lidar (DIAL). Here the absorption of laser light is compared at the center and far from the absorption line of an impurity in question. A measurement of differential absorption then allows one to infer the concentration of the impurity. There are many possible configurations. First there can be a two point path measurement or a measurement at a single point where a remote reflector has been placed. For either of these, there has to be a cooperative position remote from the laser. Secondly, the reflection can be from some typographical object, a building, tree or hillside. Since the reflection is diffuse, this second approach generally requires more transmitted power. In either case, what one ends up with is path integrated concentration of the impurity. A third approach is to use the existing atmospheric aerosols as the scattering mechanism. Here the impurity concentration can be range resolved, but the transmitted power requirement is larger still. Furthermore, since the reflector is rough and the propagation is affected by atmospheric turbulence, the measurement is only meaningful when averaged over a large number of laser pulses.

There are many possible impurities which could be detected with IR DIAL, but the field is hampered by a lack of tunable, powerful lasers. To quote Fredriksson [58]"DIAL applications in the mid-IR region in general, suffer from lack of tunable, high energy laser sources, and detection techniques is so far not as highly dedicated as in the UV and visible DIAL technique. ..... A great deal of effort has been put into IR DIAL techniques by many research groups, but it is somewhat discouraging that so few field measurements have been made. However everything points to a breakthrough when well suited lasers an dedicated detection techniques become available."

In the infrared, the available sources are basically line tunable sources. Thus DIAL measurements have to be the result of a coincidence between one of the available laser lines and the absorption line of the impurity in question. For a CO_2 laser, the lines are separated by about 50 GHz, while the atmospheric line widths

are typically 2-3 GHz. Thus, most of the spectral region between 9 and 11 μm is uncovered. For the case where there is a coincidence of lines, one can do DIAL measurements. For instance Killinger an Menyuk[59] used a CO_2 laser DIAL system, where the reflected beam was from a typographic object, to detect CH_4. Shown in Fig. (23), taken from Ref.(59) are the absorption as a function of inverse wave length for air with and without 40 ppb of CH_4. Note the coincidence of the absorption peak of CH_4 with the P(14) line of the CO_2 laser. With their DIAL setup and reflections from a typographic object, concentrations as low as 10 parts per billion were detected over both roads and airplane runways. Their maximum range was about 2.7 km. The use of a fielded infrared FEL would open the capability of IR DIAL, but without relying on coincidences between the particular laser and the absorption line of the impurity in question. In addition its continuous tunability would allow not only for measurements at two wavelengths, on and off the absorption line; but would also allow for full resolution of the spectral line shape.

In addition to its tunability, the FEL also brings an increase in radiated power by many orders of magnitude, as is apparent from Fig.(2). This is especially true between about 3 and 9 μm wavelength, and over a larger range still if one considers continuously tunable power. In DIAL, the maximum range scales as the transmitted power squared, since all of the radiated beam intersects the target. Thus FEL's have the capability of greatly increasing the range of DIAL systems. These ranges are currently rather short, hundreds of meters to a few kilometers, and integration times are correspondingly long. For instance Weitkamp[60] et al measured HCl concentration as a function of distance from an incineration ship by using a low power DF DIAL laser system. His results, taken from Ref.(60) are shown in Fig. (24). The integration time for each plot was about an hour, and the maximum range for the system was about 2 km. Thus if FEL's with average power of order 100 Watts could be fielded, the entire area of IR DIAL could be ripe for a breakthrough.

VII. Conclusion

Gyrotrons and FEL's have potential for greatly increasing the capability of atmospheric sensors. They could extend weather radars and lidars to new regimes of power, wavelength and tunability. Gyrotron oscillators at 94 GHz, and quasi-optical gyrotron oscillators or amplifiers could be fielded today. It is possible that more conventional gyrotron amplifiers at this frequency will soon be available also. The development of FEL's has not yet matured to the point where they could be fielded, however there are several development strategies that could lead in this direction.

Acknowledgement

The author would like to thank R. Lhermitte, D. Atlas, M. Sundquist, T. Ackerman, R. Presutti, J Stanley, N. Menyuk, and A. Fliflet for a number of very useful discussions. The calculation in Fig 6 was done by A. Fliflet. This work was supported by ONR.

References:

1. H. Liebe, Int. J. IR and Millimeter Waves, 10, 631, (1989)

2. D. Killinger and N. Menyuk, Science, 325, 37, (1987)

3. K. Kresicher and R. Temkin, Phys. Rev. Let,. 59. 547, 1987

4. K. Kreischer et al, Phys Fluids B2, 640, 1990

5. A. Gaponov et al, Int. J. Electronics, 51, 277, 1981

6. A. Fix et al, Int. J. Electronics, 57, 821, 1984

7. A. Bensimhon, G. Faillon, G. Garin, and G. Mourrier, Int. J. Electronics, 57, 805, 1984

8. E. Borie et al, 15th IR and Millimeter Waves Conference, Temkin ed, SPIE Vol 1514, p493, 1990

9. Y. Mitsunaka et al, 15th IR and Millimeter Waves Conference, Temkin, ed, SPIE Vol 1514, p318, 1990

10. H. Guo et al, IEEE Trans. Plasma Sci., 18, 326, 1990

11. A. Fliflet et al, J. Fusion Energy, 9, 31, 1990

12. K. Felch et al, Int. J. Electronics, 57, 815, 1984

13. K. Felch et al, Int. J. Electronics, 61, 701, 1986

14. V. Flyagin, A. Goldenberg, and V. Zapevalov, 18th International Conference on IR and MM Waves, Colchester, England, September, 1993, SPIE Vol 2104, p 581

15. G. Bergeron, M. Czarnaski, and M. Rhinewine, Int. J. Electronics, 69, 281, 1990

16. M Rhinewine et al, 15th IR and Millimeter Waves Conference, Temkin ed, SPIE Vol 1514, pp 578, 1990

17. I.I. Antakov, E.V. Zasypkin, and E. Sokolov, 18th International Conference on IR and MM Waves, Colchester, England, September, 1993, SPIE Vol 2104, p 466

18. A. Fliflet, R. Fischer, and W. Manheimer, Phys. Fluids B, 5, 2682, (1993)

19. R. Fischer et al, Phys. Rev. Let. to be published, 1994

20. G. Scheitrum, T. Bemis, T. Hargreaves, and L. Higgens, 18th International Conference on IR and MM Waves, Colchester, England, September, 1993, SPIE Vol 2104, p 523

21. T. Hargreaves, K. Kim, J. McAdoo, S. Park, R. Seeley, and M. Read, Int. J. Electronics, 57, 977, 1984

22. A. W. Fliflet, T. Hargreaves, W. Manheimer, R. Fisher, M. Barsanti, B. Levush, and T. Antonsen, Phys Fluids, B2, 1046, 1990

23. A. Fliflet, T. Hargreaves, W. Manheimer, R. Fisher, and M. Barsanti, IEEE Trans Plasma Sci, 18, 306, 1990

24. T. Hargreaves, A. Fliflet, R. Fisher, M. Barsanti, W. Manheimer, B. Levush, and T. Antonsen, Int. J. Electronics, 72, 807, 1992

25.. S. Alberti, M. Podrozzi, M. Tran, J. Hogge, T. Tran, P. Muggli, H. Jodicke, and H. Mathews, Phy. Fluids B, 2, 2544, (1990)

26. R. Adler, Proc. IRE, 34, 351, (1946)

27. G. Ramian, in *Short Wavelength Radiation Sources*, P. Sprangle ed, Proc. SPIE 1552, 57, (1991)

28. M. Sundquist, private communication, July, 1992

29. W. Manheimer and A. Fliflet, IEEE J. Quantum Electronics, to be published, 1994

30. K.D. Chan, K. Meier, D. Nguyen, R. Sheffield, T. Wang, R. Warren, W. Wilson, and L. Young, in *Short Wavelength Radiation Sources*, P. Sprangle ed, Proc. SPIE 1552, 69, (1991)

31. D. Feldman, R. Warren, W. Stein, J Fraser, G. Spalek, A. Lumkin, J. Watson, B. Carlsten, H. Takeda, and T. Wang, Nucl. Instr. Meth. Phys. Res. A259, 26, (1987)

32. T. Smith,H. Schwettman, R. Rohatgi, Y. Lapierre, and J. Edighoffer, Nucl. Instr. Meth. Phys. Res. A259, 1, (1987)

33. G. Zorpette, EEE Spectrum, 30, 21, July, 1993

34. R. Lhermitte, J. Atmospheric and Oceanic Tech. 4, 36, 1987

35. R. Lhermitte, IEEE Trans. Geoscience and Remote Sensing, 26, 207, 1988

36. R. Lhermitte, Geophysical Res. Lett., 14, 707, 1987

37 R. Lhermitte, Geophysical Res. Lett., 15, 1125, 1988

38. T. Ackerman, private communication, September, 1993

39. M. Skolnik, *Introduction to Radar Systems,* McGraw Hill, 1980, p 369

40. W. Manheimer, Int. J. Electronics, 72, 1165, (1992)

41. Ref 39, 106

42. D. Atlas, private communication, September, 1993

43. D. Atlas, GEWEX Workshop on Cloud Radar, June 1993, JPL, Pasadena, CA

44. Yu. Bekov, Yu. Dryagin, L. Kukin, and M. Tokman, Radio Physics and Quant. Electronics, to be published, 1994

45. Doviak and Zrnic, Chapters 10 and 11

46. R. J. Hill J. Fluid Mechanics, 88, 541, 1978

47. V.I. Tatarskii, *Effects of the TurbulenceAtmosphere on Wave Propagation*, Available from US Dept Commerce, UDC 551.510, ISBN, 07065 0680 4 Natl. Tech. Inf. Service, Springfield, VA

48. R.M. Price, *Radiometer Fundamentals*, in *Methods of Experimental Physics 12B*, M. Meeks, ed, p 201, Academic Press, 1976

49. J. Waters, *Absorption and Emission by Atmospheric Gases*, in *Methods of Experimental Physics 12B*, M. Meeks ed, p 142, Academic Press, 1976

50. J. Waters, Proc, IEEE, 80, 1679. (1992)

51. A. Randegger, Pure and Applied Geophys. 118, 1052, 1980

52. A. Parrish, R. deZafra, P. Soloman, and J. Barrett, Radio Science, 23, 106, 1988

53. J. Waters, L. Froidevaux, W. Read, G. Manney, L. Elson, D. Flower, R. Jarnot, and R. Harwood, Nature, 362, 597, (1993)

54. N. Menyuk, D. Killinger, and C. Menyuk, Applied Optics, 21, 3377, (1982)

55. R. Presutti, Private communication, October, 1992

56. J. Stanley, Private communication, October, 1992

57. R. Measures ed, *Laser Remote Chemical Analysis*, J. Wiley, (1988)

58. K. Fredriksson, Chapter 4, Ref 57

59. D. Killinger and N. Menyuk, IEEE J. Quantum Electronics, QE17, 1917, (1981)

60. C. Weitkamp, in *Wastes in the Ocean*, Vol 3, Wiley, New York, 1981

Table 1 — Capabilities of recent Russian gyrotrons at about 94 GHz.

RUSSIAN GYROTRONS AT ABOUT 94 GHZ WITH GAUSSIAN MODE OUTPUT STRUCTURE

Frequency GHz	Power (MW)	Pulse Duration (s)	Efficiency %
83	0.5	1.5	37
110	0.5	1.5	35
140	0.9	0.3	36
167	0.5	0.7	30

Table 2 — Possible applications of 94 GHz radars to cloud studies.

SHORT COMPENDIUM OF 94 GHZ RADAR APPLICATIONS
DAVID ATLAS

* RADAR STUDIES OF SEEDED ATMOSPHERE WITH NONPERTURBING CHAFF

* RELIABLE DETECTION OF CLOUD BASES AND TOPS

* SORTING OUT PRECIPITATION MECHANISMS IN WATER AND ICE CLOUDS

* LIFETIME OF PRECIPITATING CELLS

* RADAR STALACTITES AND MAMMATA AT BASE OF ICE CLOUDS

* FIRST ECHO STUDIES; EARLY DEVELOPMENT OF CLOUDS AND STORMS

* FLOW IN YOUNG CONVECTIVE CLOUDS; EFFECT OF TURBULENCE ON CONDENSATION

* MIXING ACROSS INVERSION LAYERS

Table 3 — Characterization of the strength of clear air turbulence.

Turbulence	$C_n^2\ m^{-2/3}$	$\varepsilon\ m^2/s^{-3}$
Weak	$6x10^{-17}$	$3x10^{-3}$
Moderate	$2x10^{-15}$	$8.5x10^{-3}$
Severe	$3x10^{-13}$	$6.8x10^{-2}$

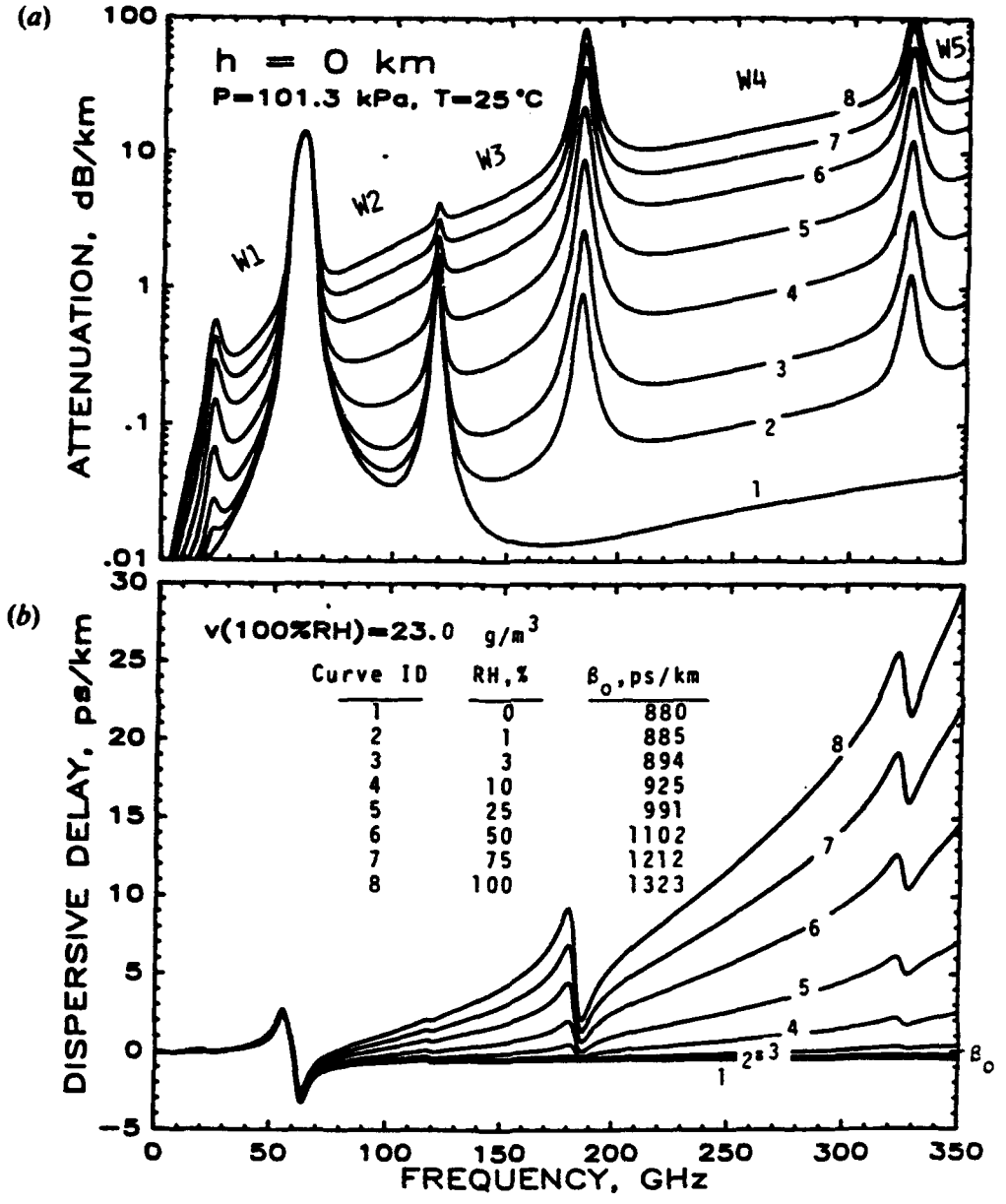

Fig. 1 — Millimeter wave atmospheric attenuation and phase shift as a function of a), frequency and b), humidity, from Ref. 1

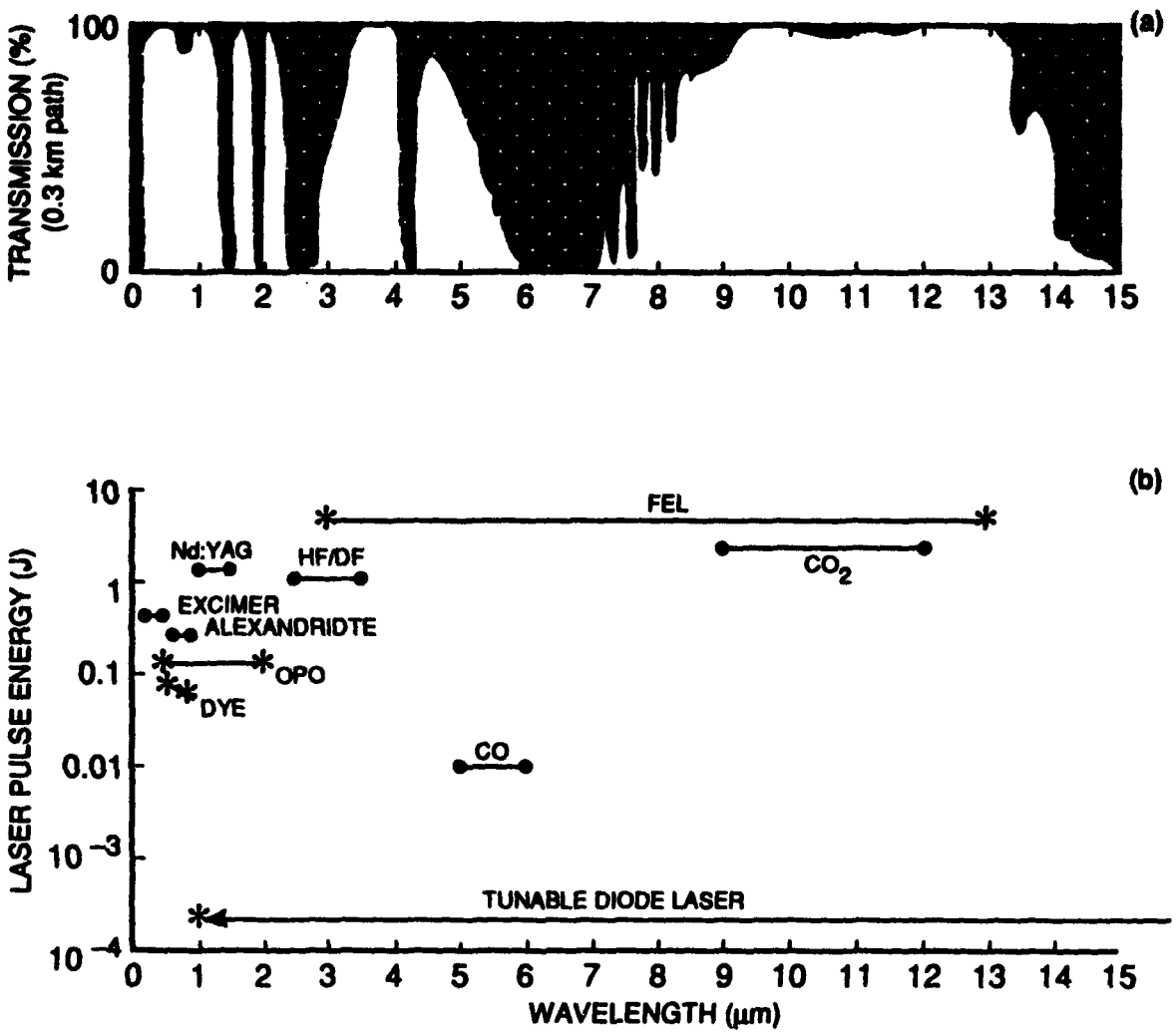

Fig. 2 — a) Atmospheric attenuation in the infrared as a function of frequency, b) Approximate capability of different laser systems. Lines ending in dots are line tunable, lines ending in stars are continuously tunable.

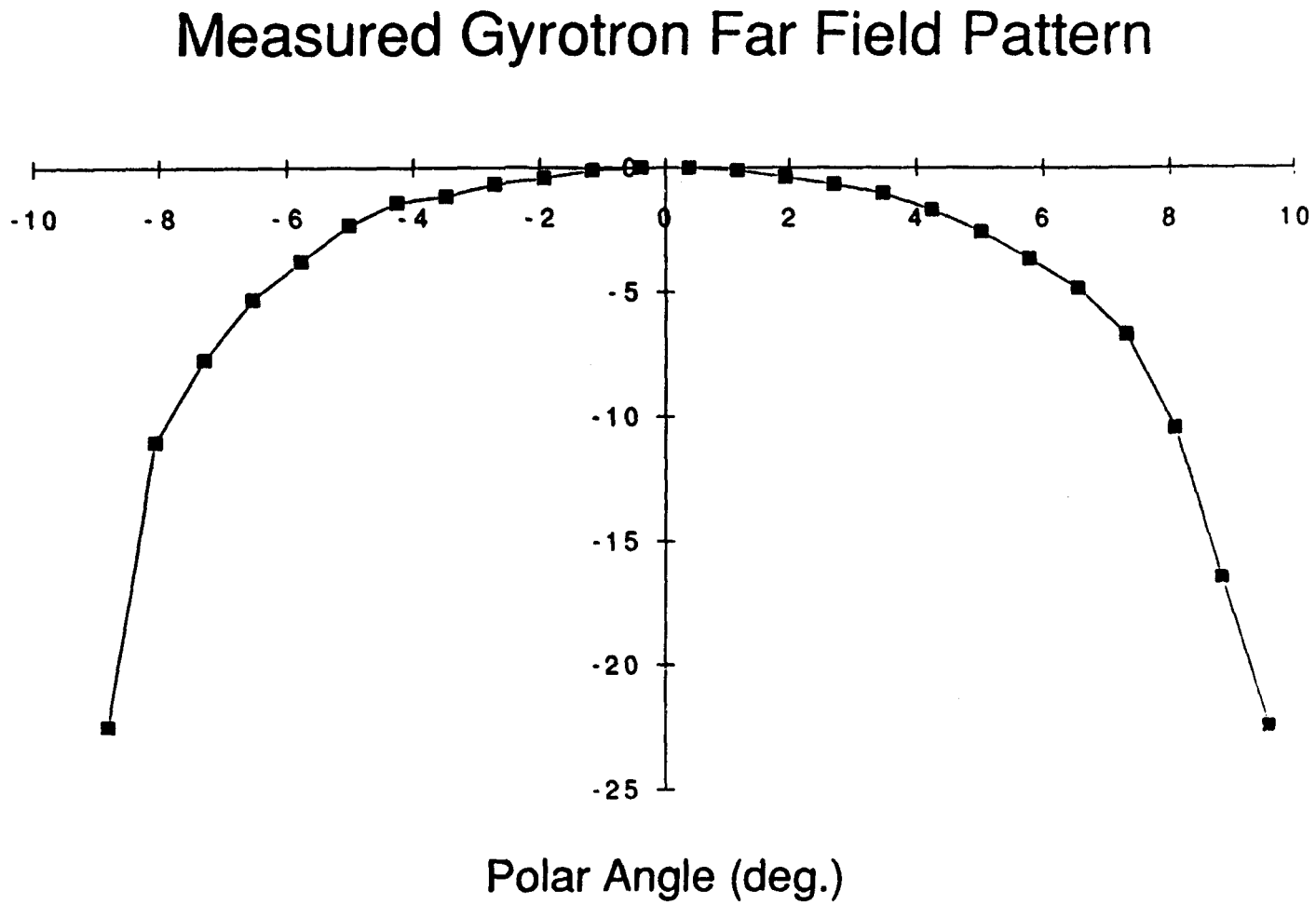

Fig. 3 — Far field mode pattern of the NRL 94 GHz gyrotron

94 GHz GYROTRON SCHEMATIC

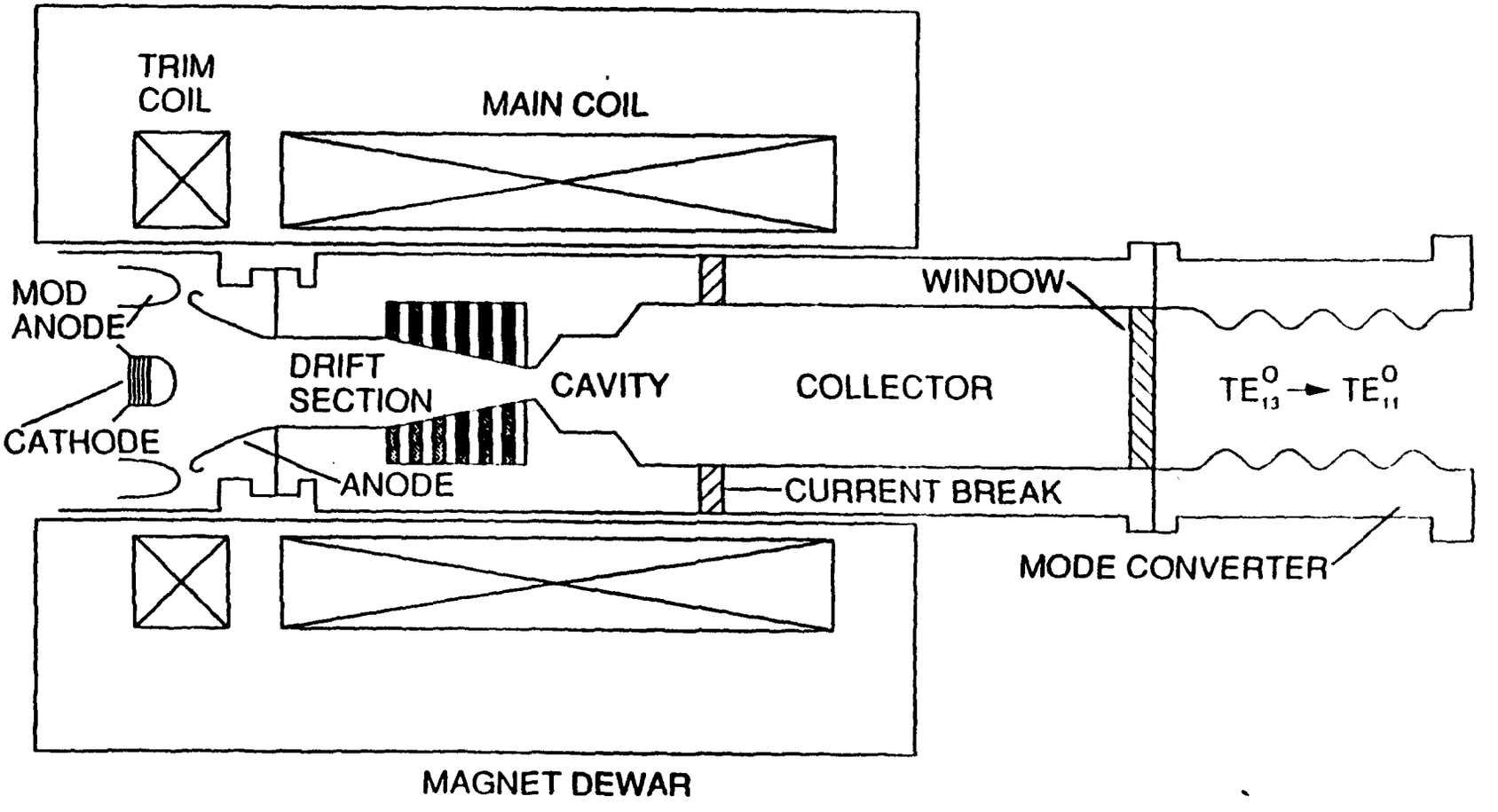

Fig. 4 — Schematic of the NRL 94 GHz TE_{13} gyrotron

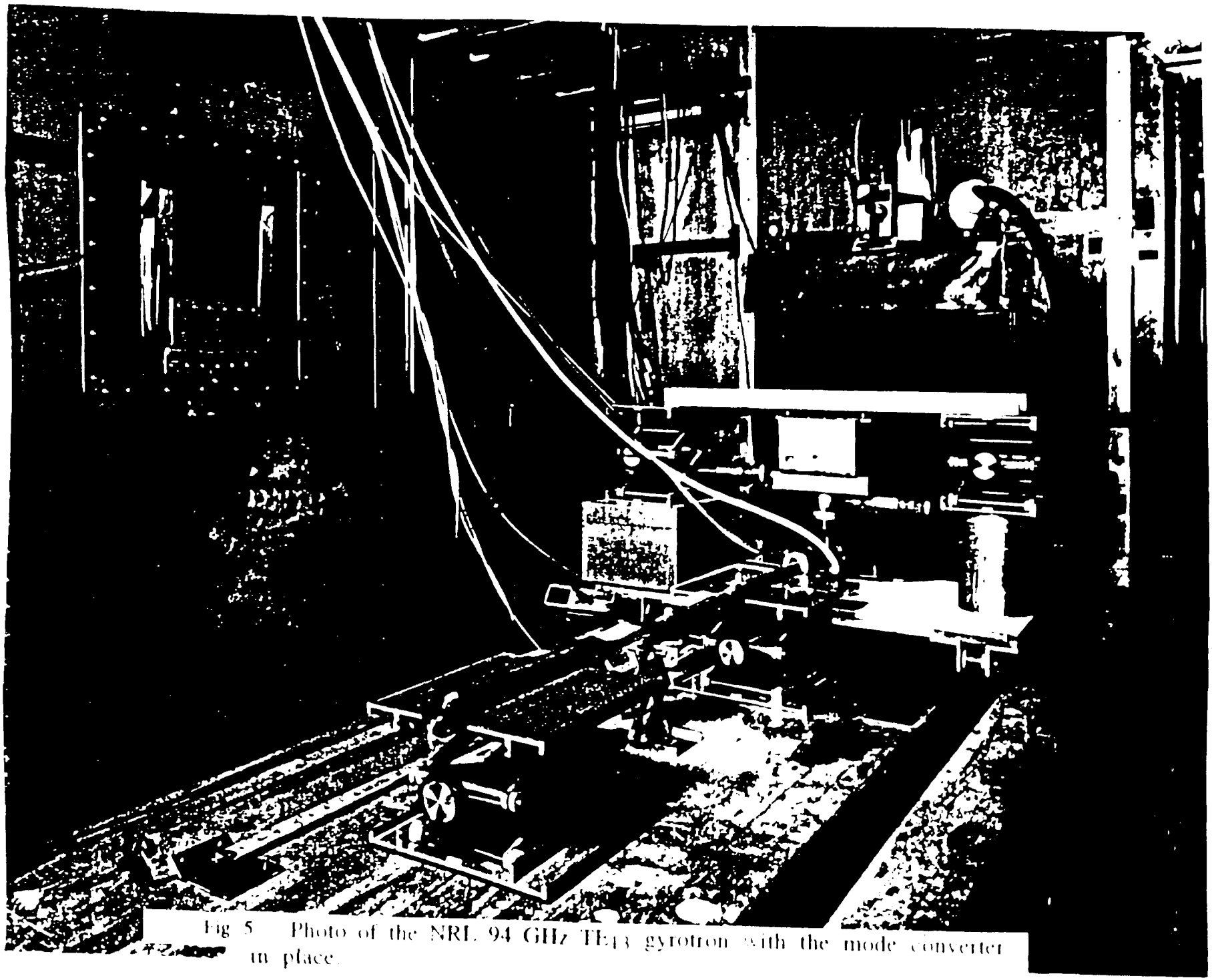

Fig 5 Photo of the NRL 94 GHz TE_{13} gyrotron with the mode converter in place.

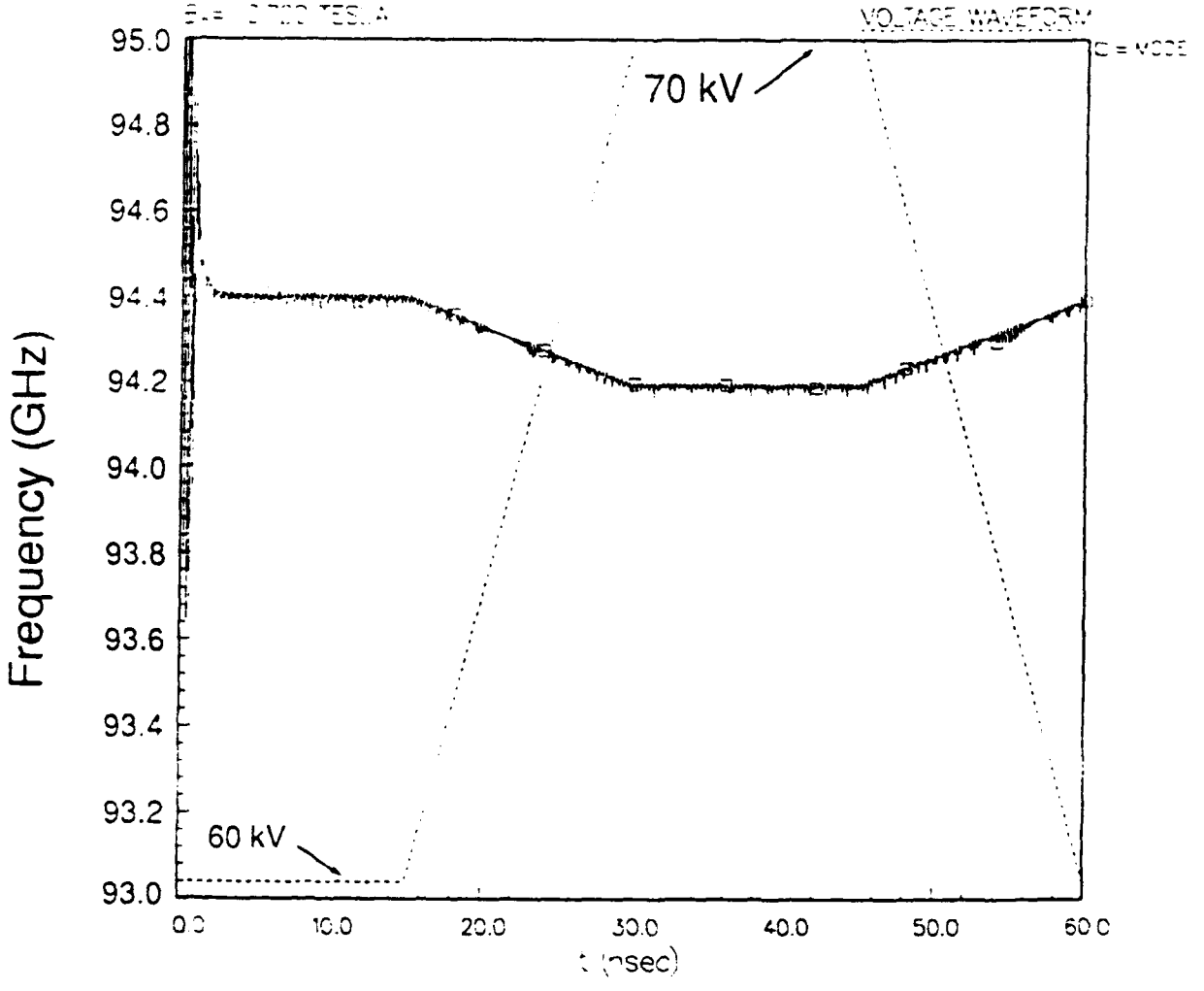

Fig. 6 — Computed plot of frequency versus time for the NRL 94 GHz gyrotron with a voltage ramp

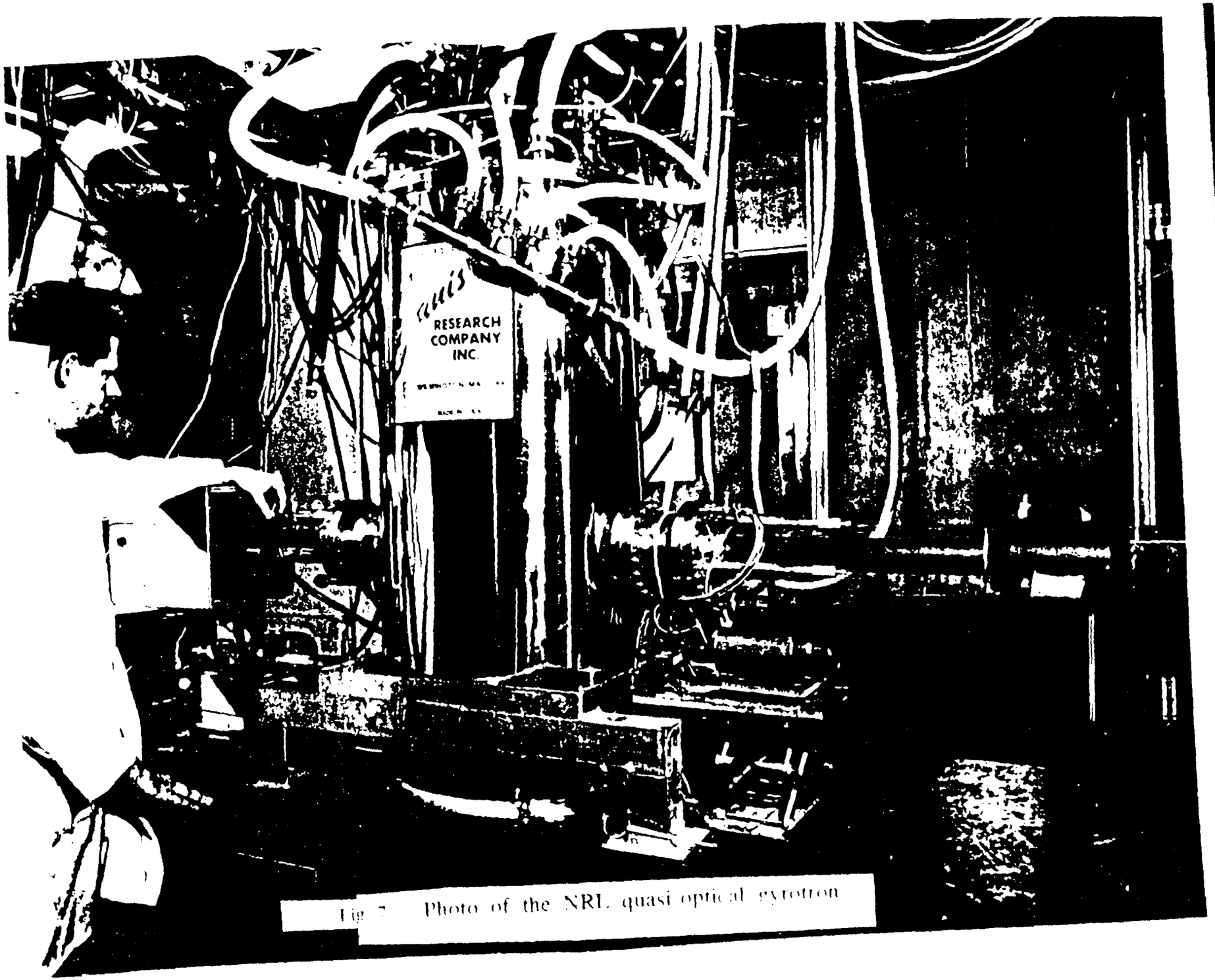

Fig. 7 — Photo of the NRL quasi-optical gyrotron

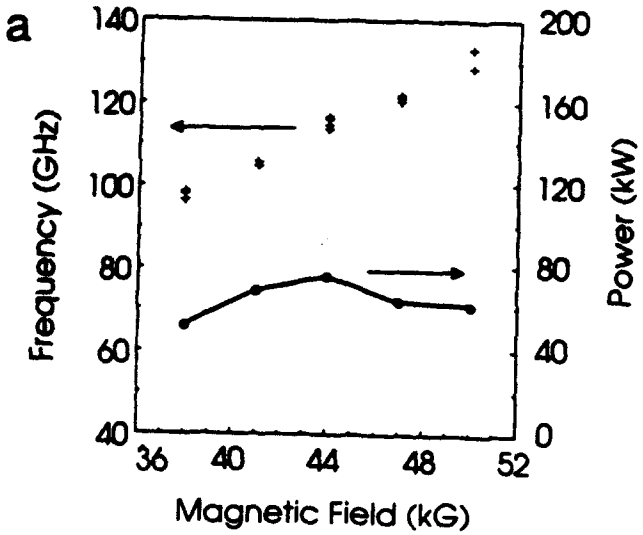

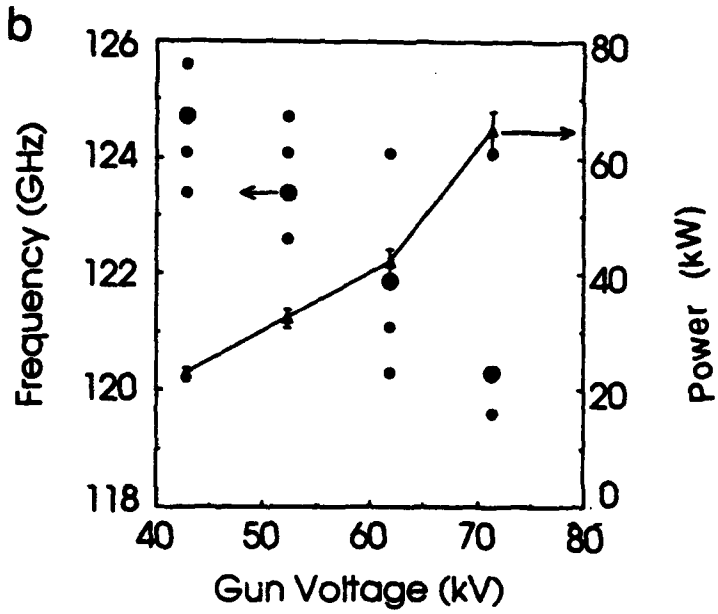

Fig. 8 — Tuning of the NRL quasi-optical gyrotron with a) magnetic field, and b) voltage

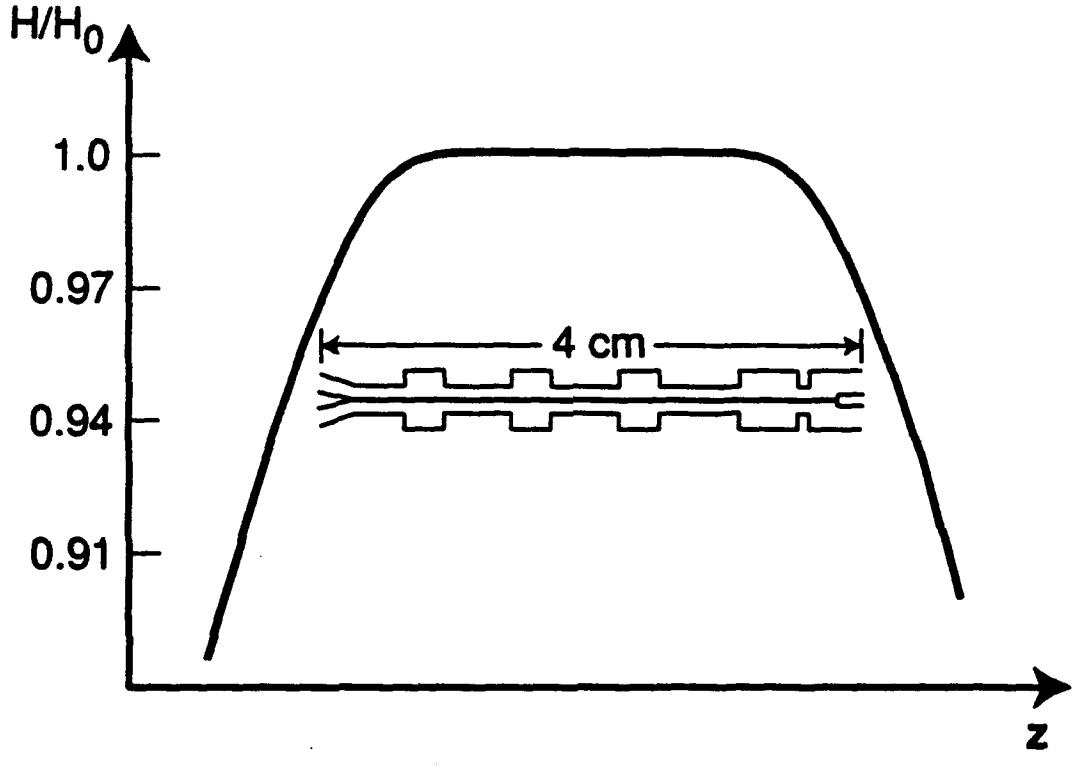

Fig. 9 — Interaction circuit for the IAP 4 cavity 94 GHz TE_{02} gyroklystron

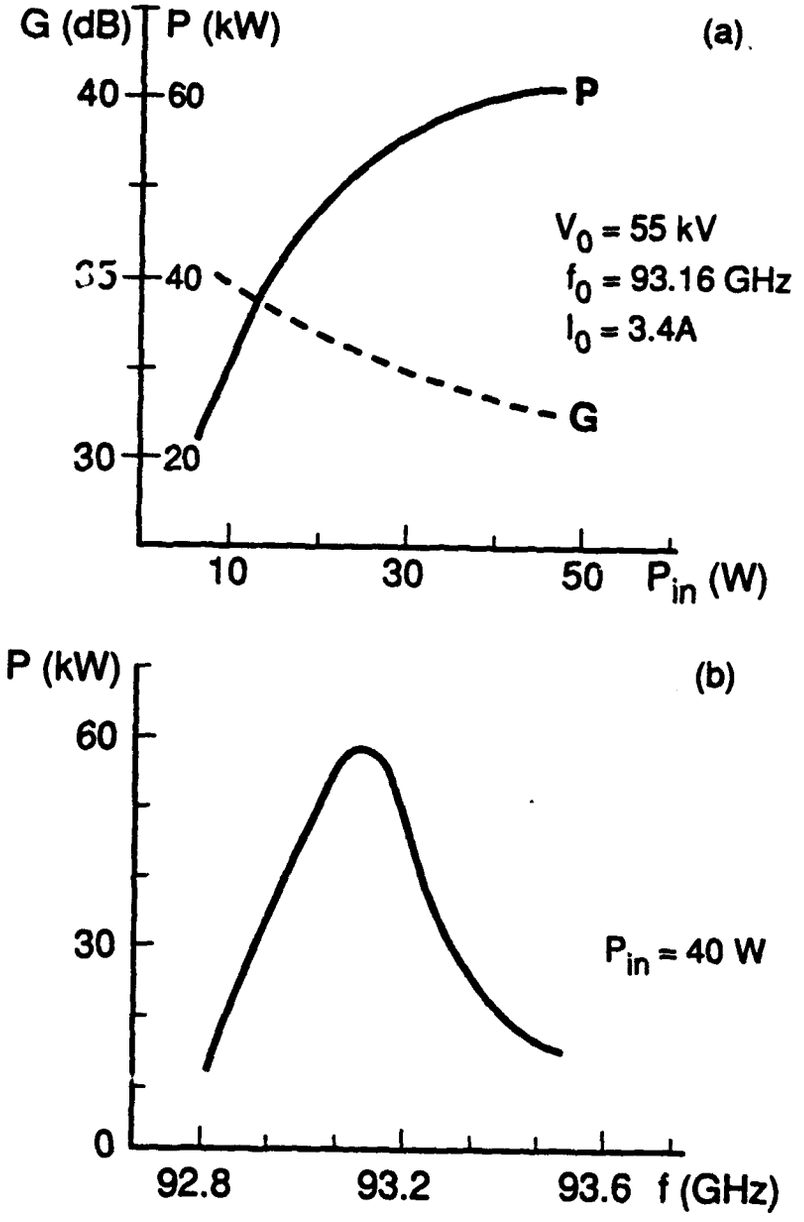

Fig. 10 — Power, gain and frequency response for the IAP 94 GHz gyroklystron

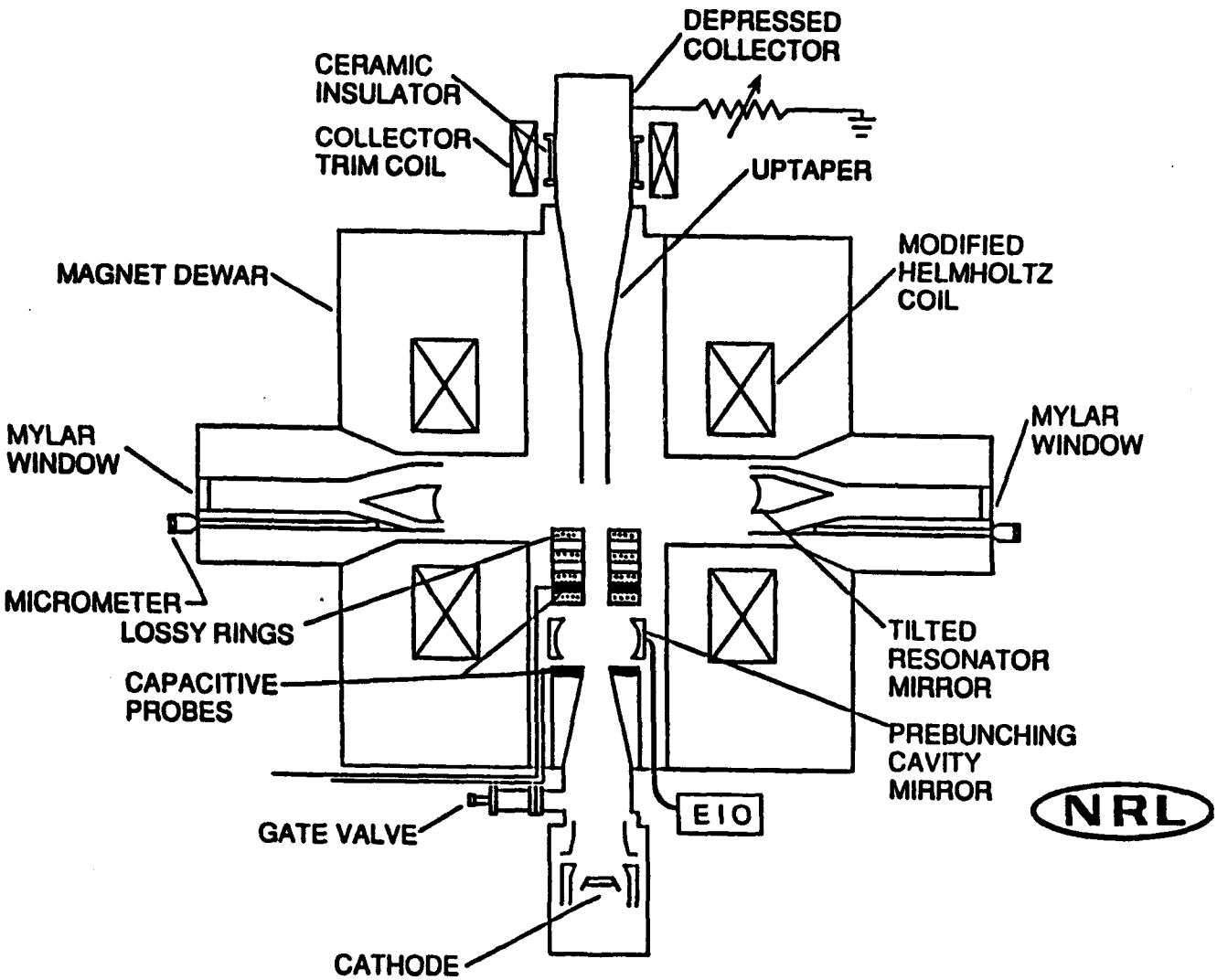

Fig. 11 — Schematic of the NRL quasi-optical gyroklystron

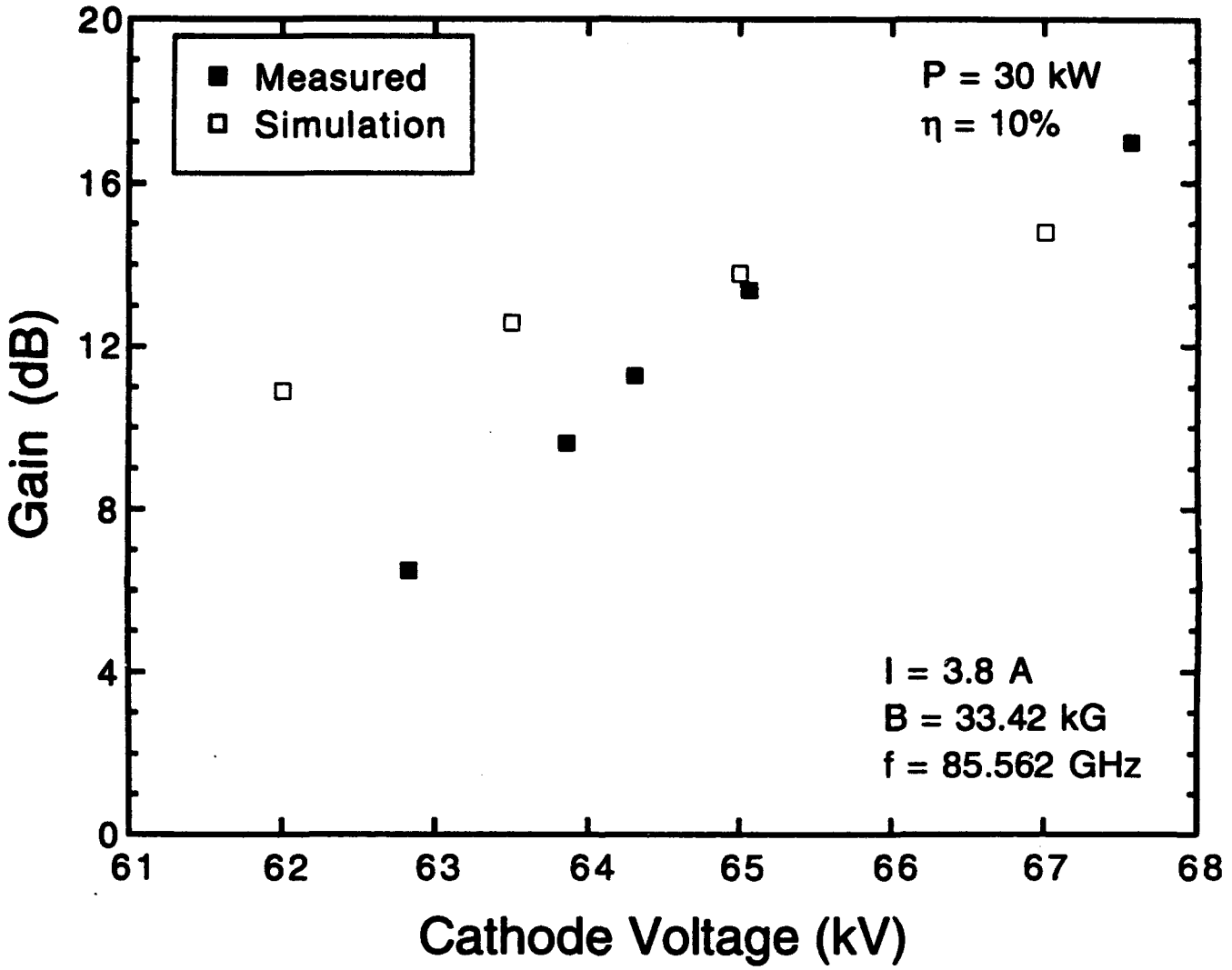

Fig. 12 — Gain as a function of cathode voltage for the NRL quasi-optical gyroklystron amplifier

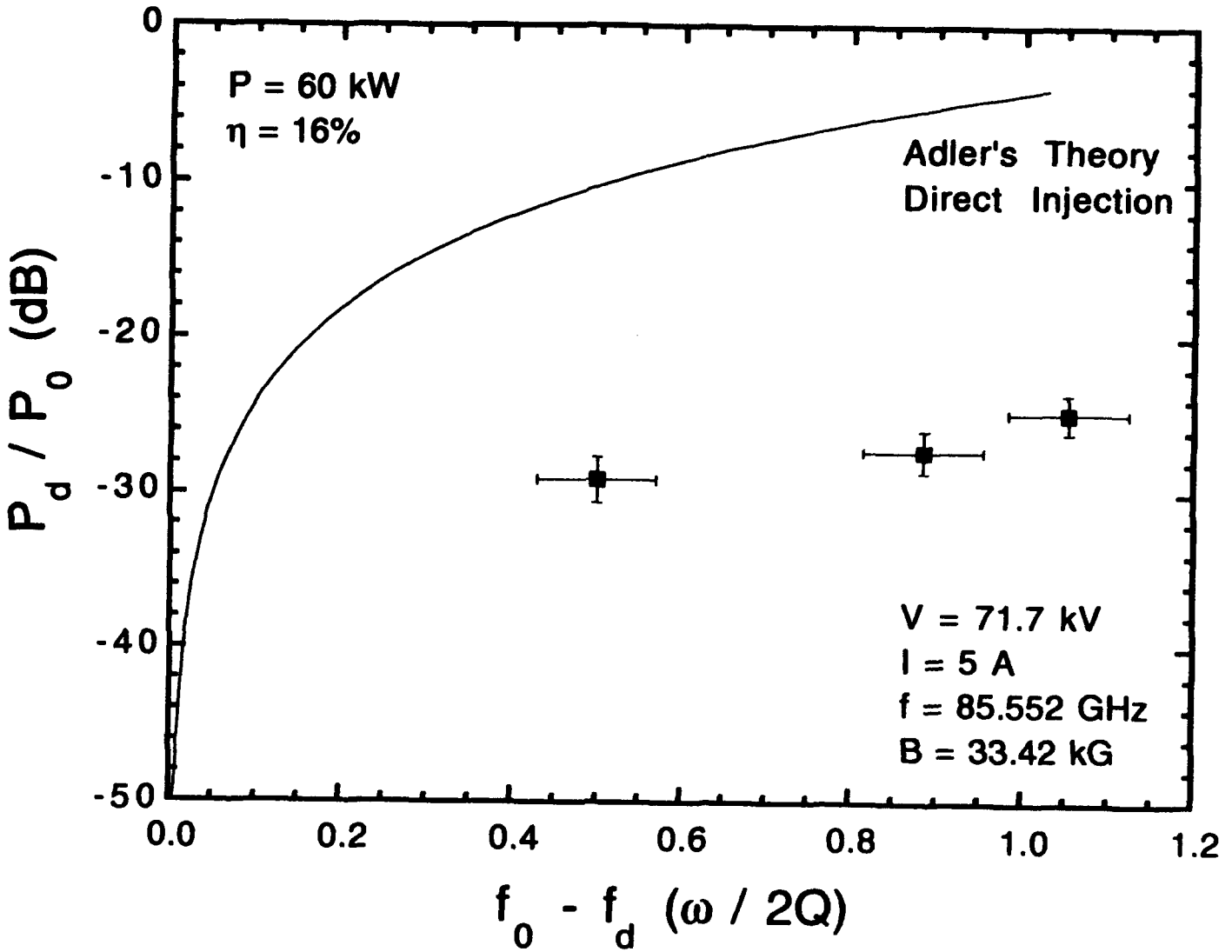

Fig. 13 — Locking bandwidth versus power ratio for the NRL quasi-optical gyroklystron phase locked oscillator

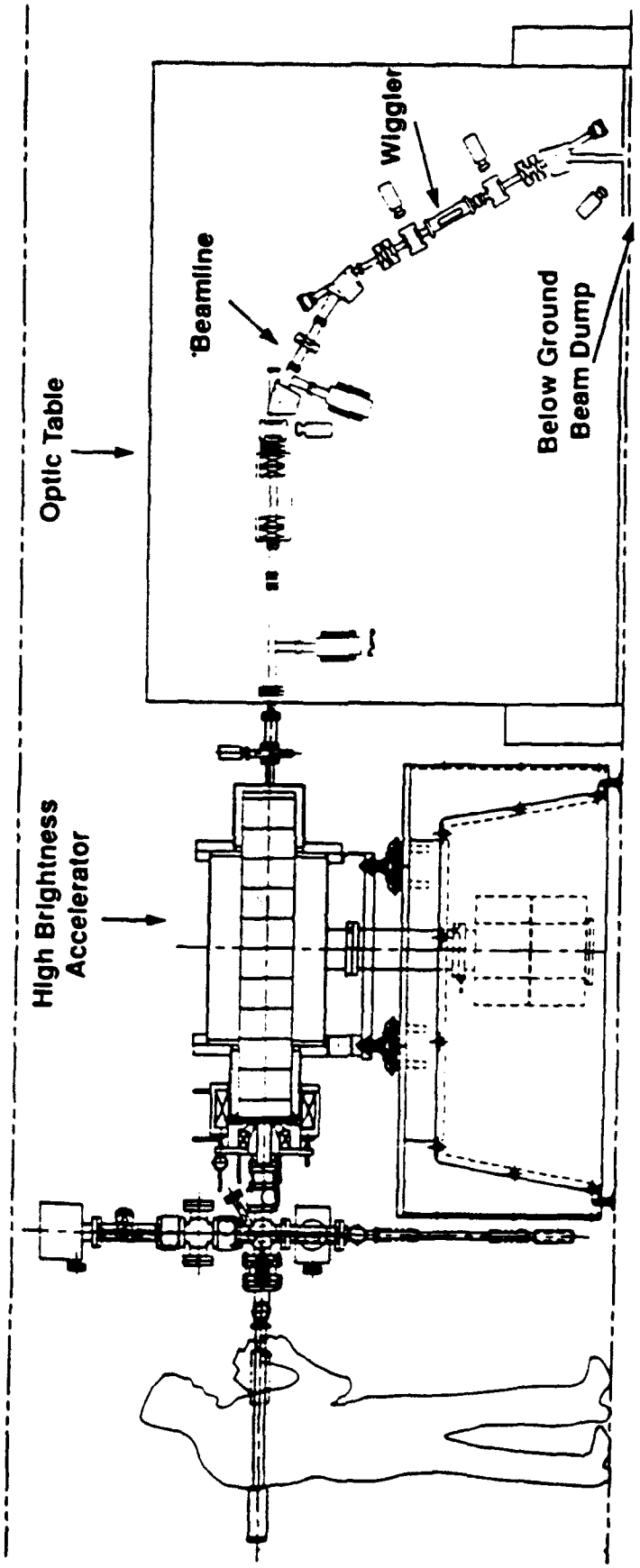

Fig. 15 — A schematic of the Los Alamos compact FEL

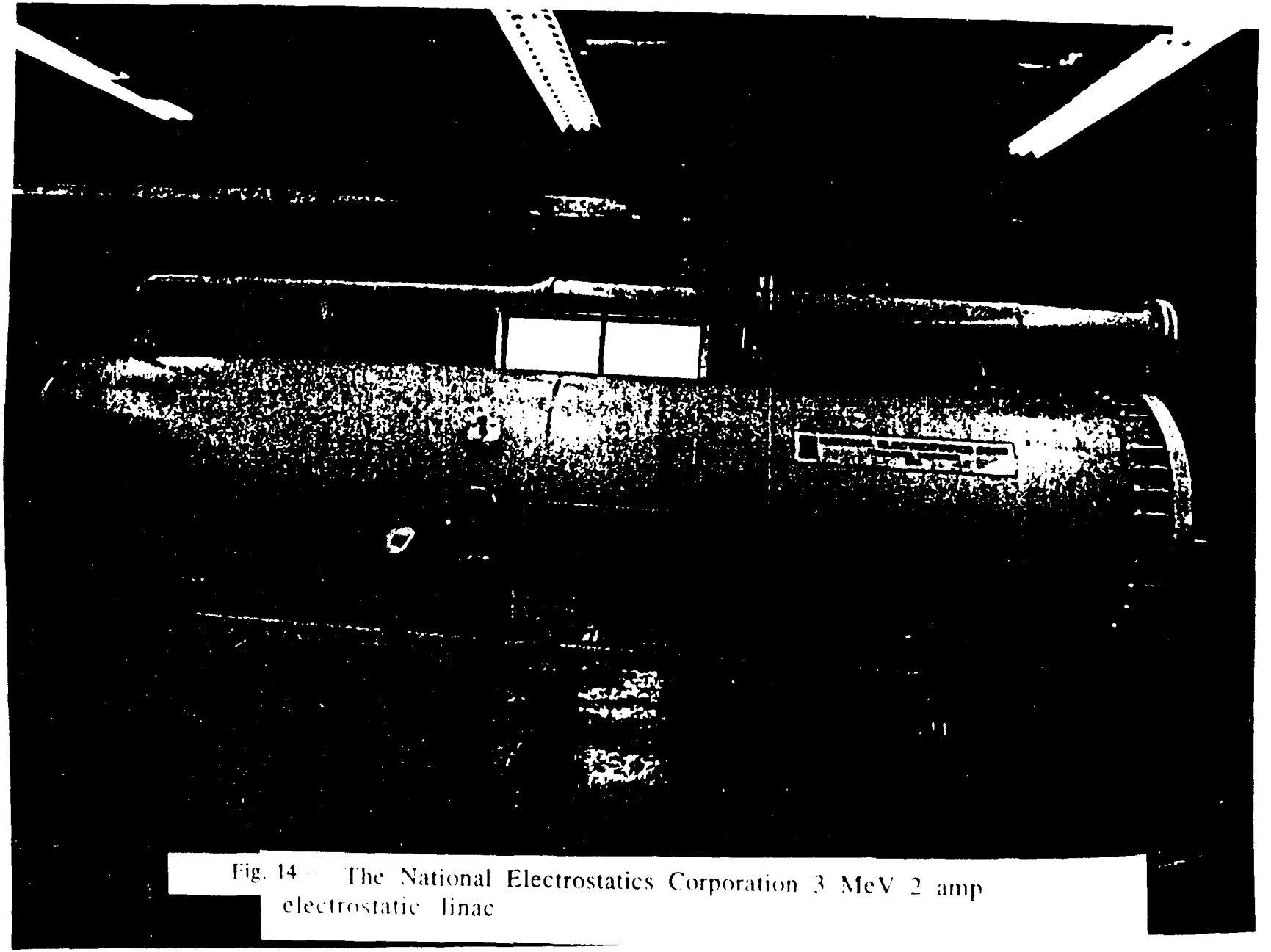

Fig. 14 — The National Electrostatics Corporation 3 MeV 2 amp electrostatic linac

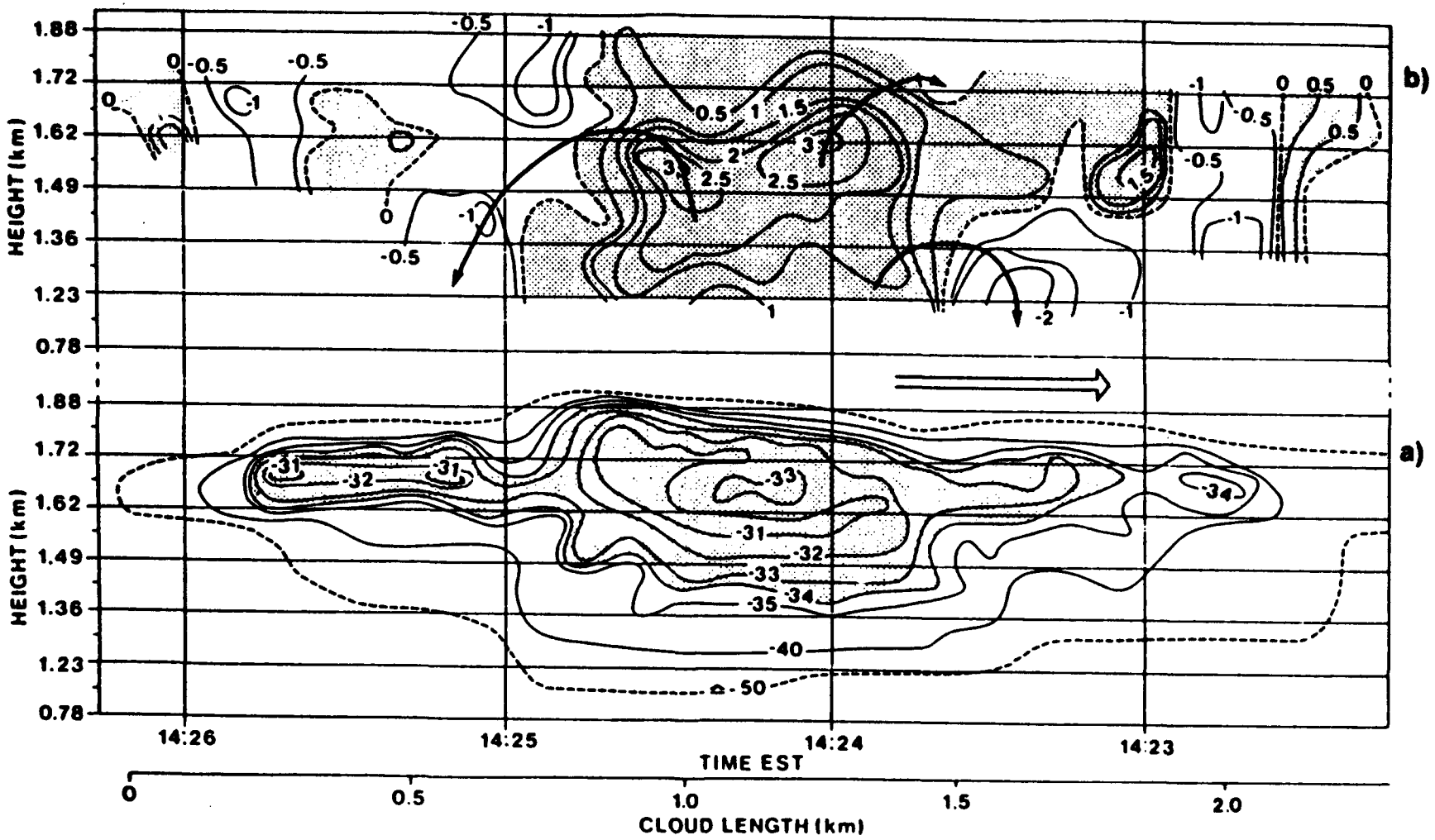

Fig. 16 — a) The reflectivity of a small cumulous cloud at 94 GHz, b) The vertical velocity on the cloud from the Doppler processing, numbers are in m/s.

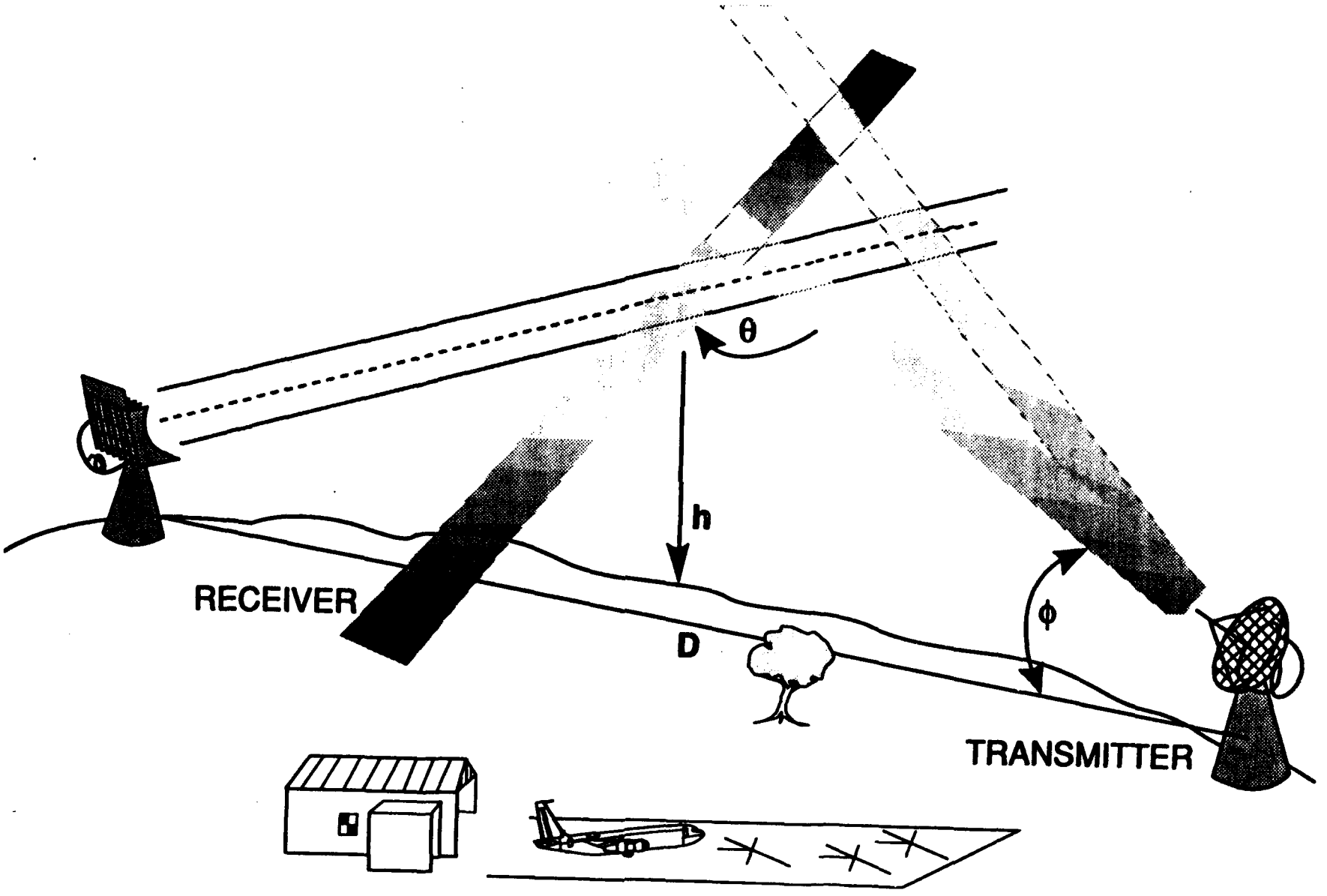

Fig. 17 — Configuration for ground based remote sensing of clear air turbulence from ground level up to an altitude of several kilometers.

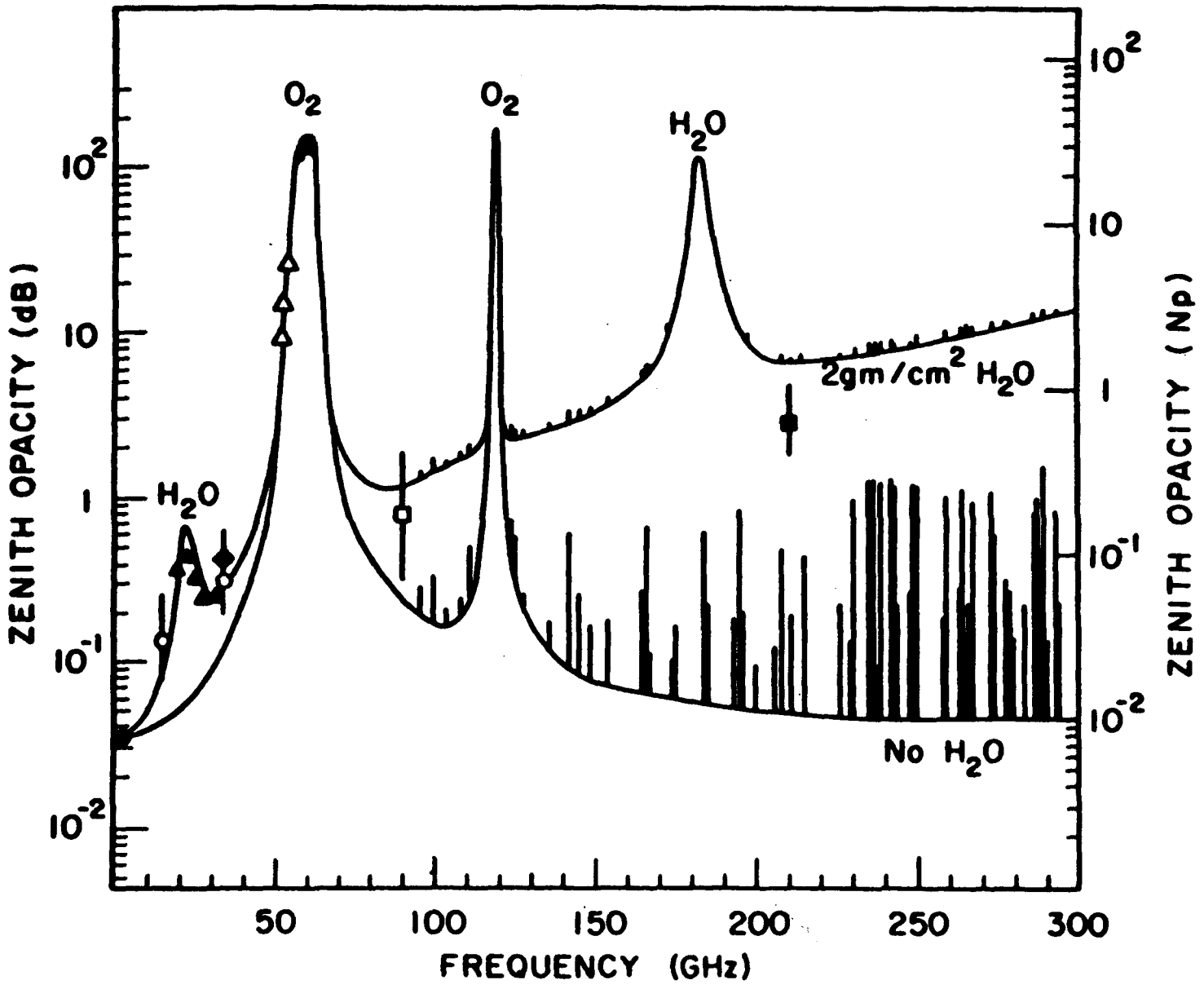

Fig. 18 — Zenith opacity of the atmosphere as a function of frequency with and without the water absorption (without water corresponds to very high altitude). The lines are the absorption due to ozone.

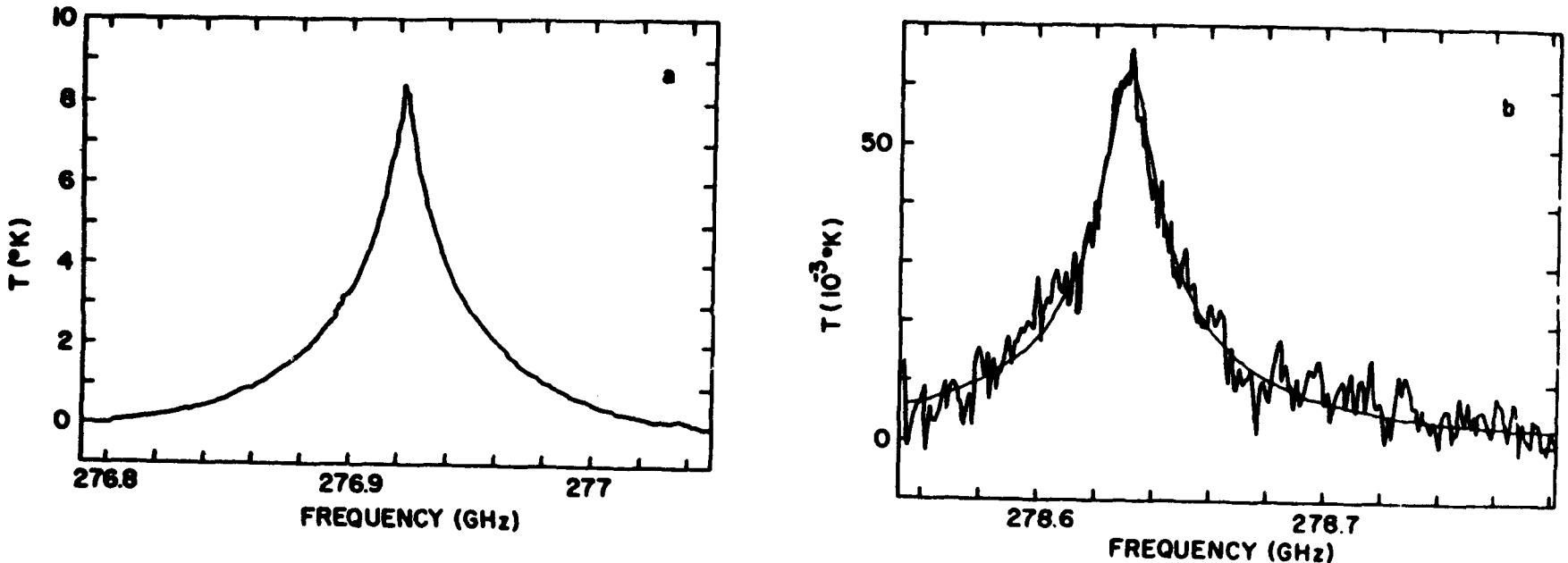

Fig. 19.— Ground based radiometer measurements of ozone and ClO from Parrish et al.

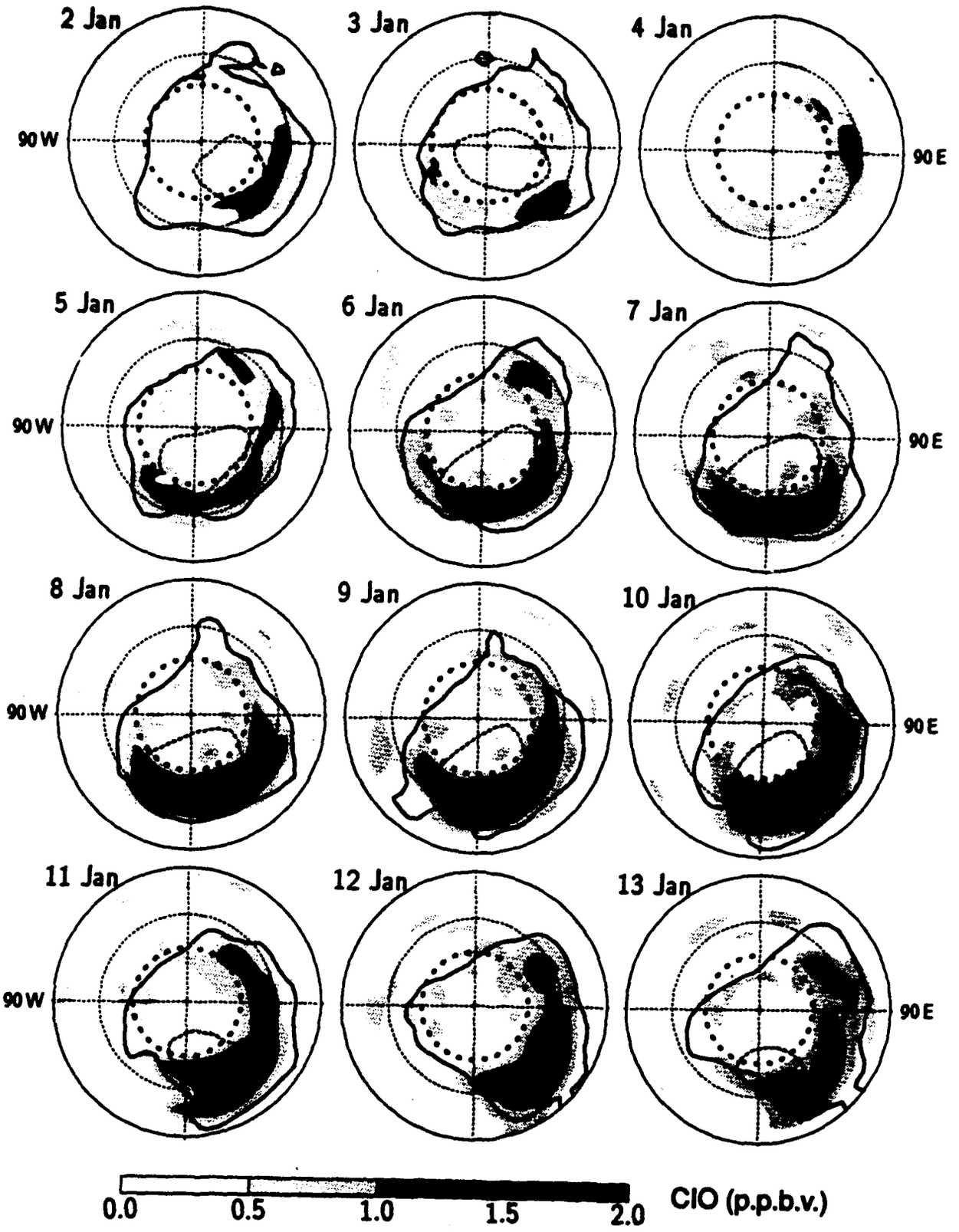

Fig. 20 — Variation in .e distribution of ClO, from Waters et al, during January 2-13, 1992 ClO abundance is indicated by the grey scale.

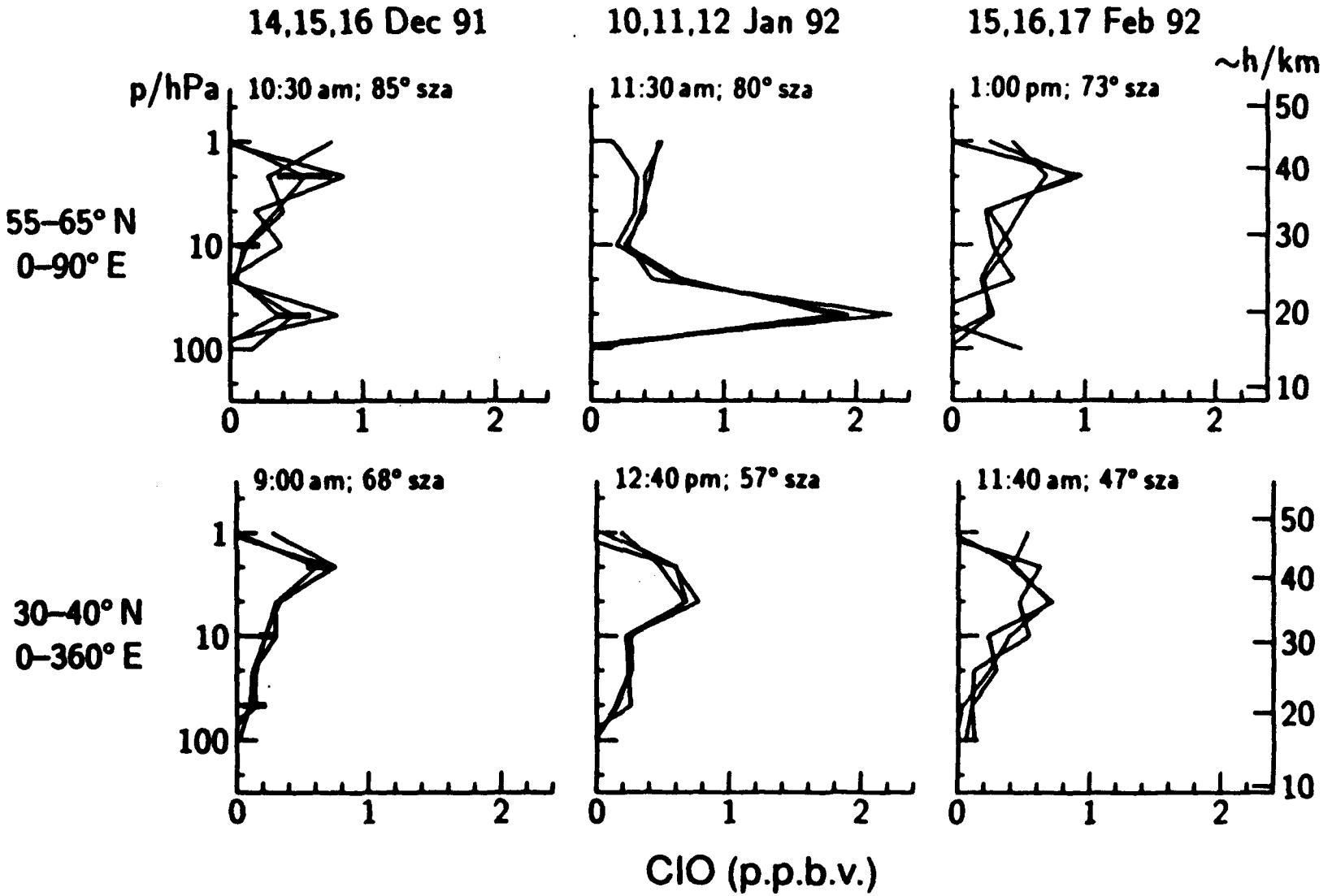

Fig. 21 — ClO vertical profiles from Waters et al. Each panel shows averages over the latitudes and longitudes indicated on the left for each of the three days. Twelve individual profiles were averaged to from the top traces, and 44 for the bottom.

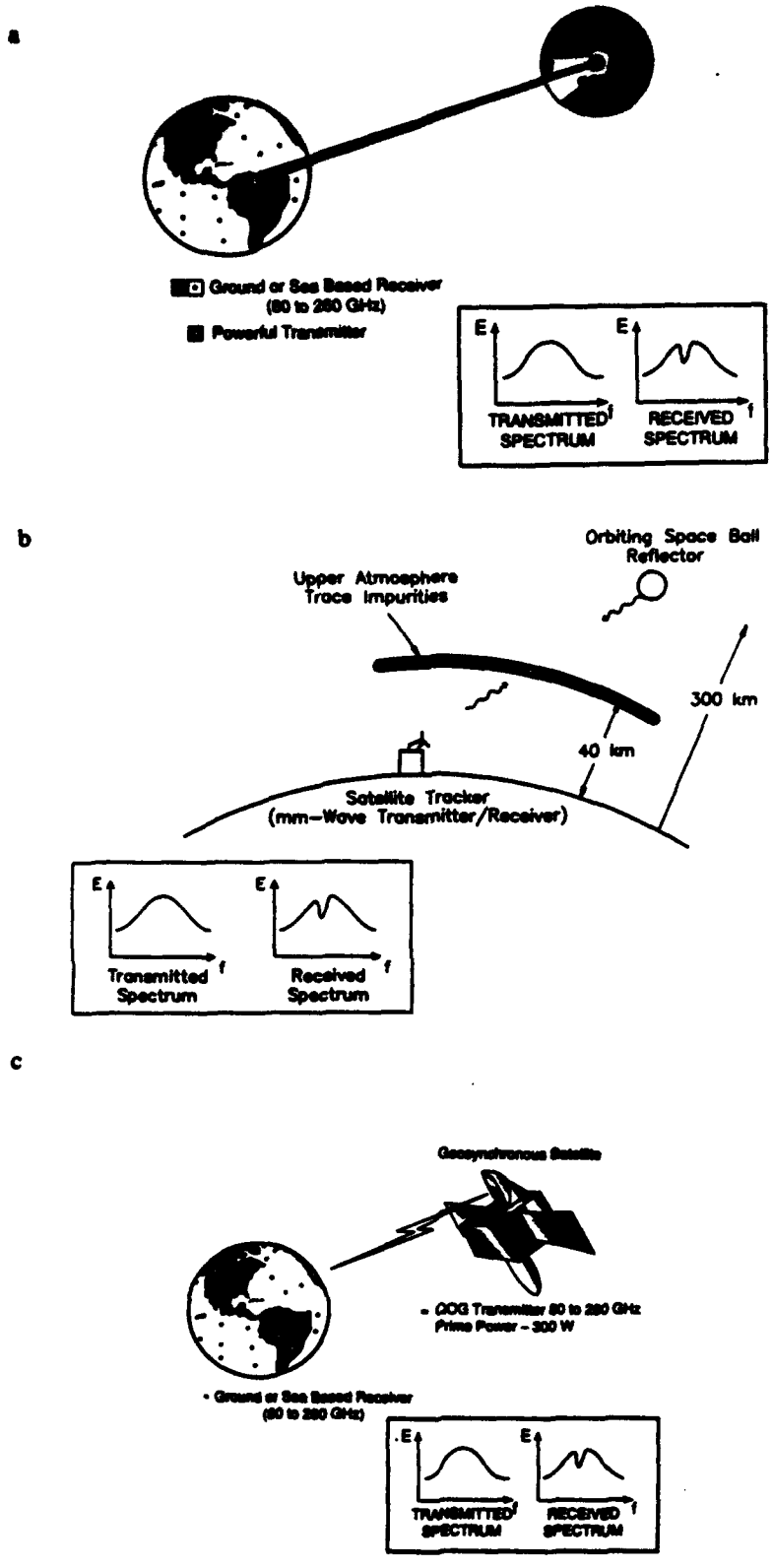

Fig. 22 — Schematic of a variety of active upper atmosphere trace element detection schemes, a) reflection from the moon, b) reflection from a spherical callibration satellite, and c) a tunable millimeter wave source in space.

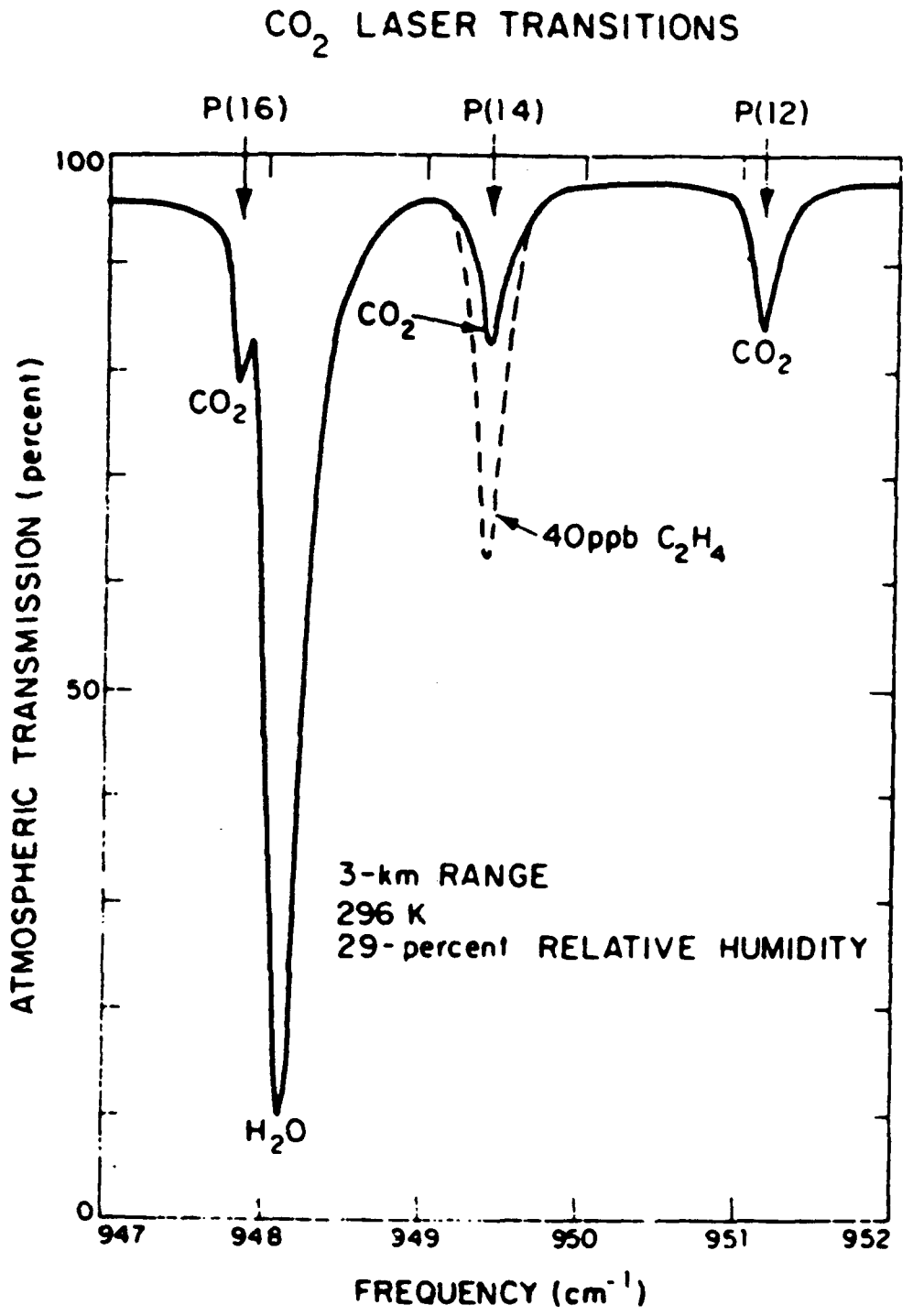

Fig. 23 — The coincidence of a CH_4 absorption line and the line of a CO_2 laser, taken from Ref. 26.

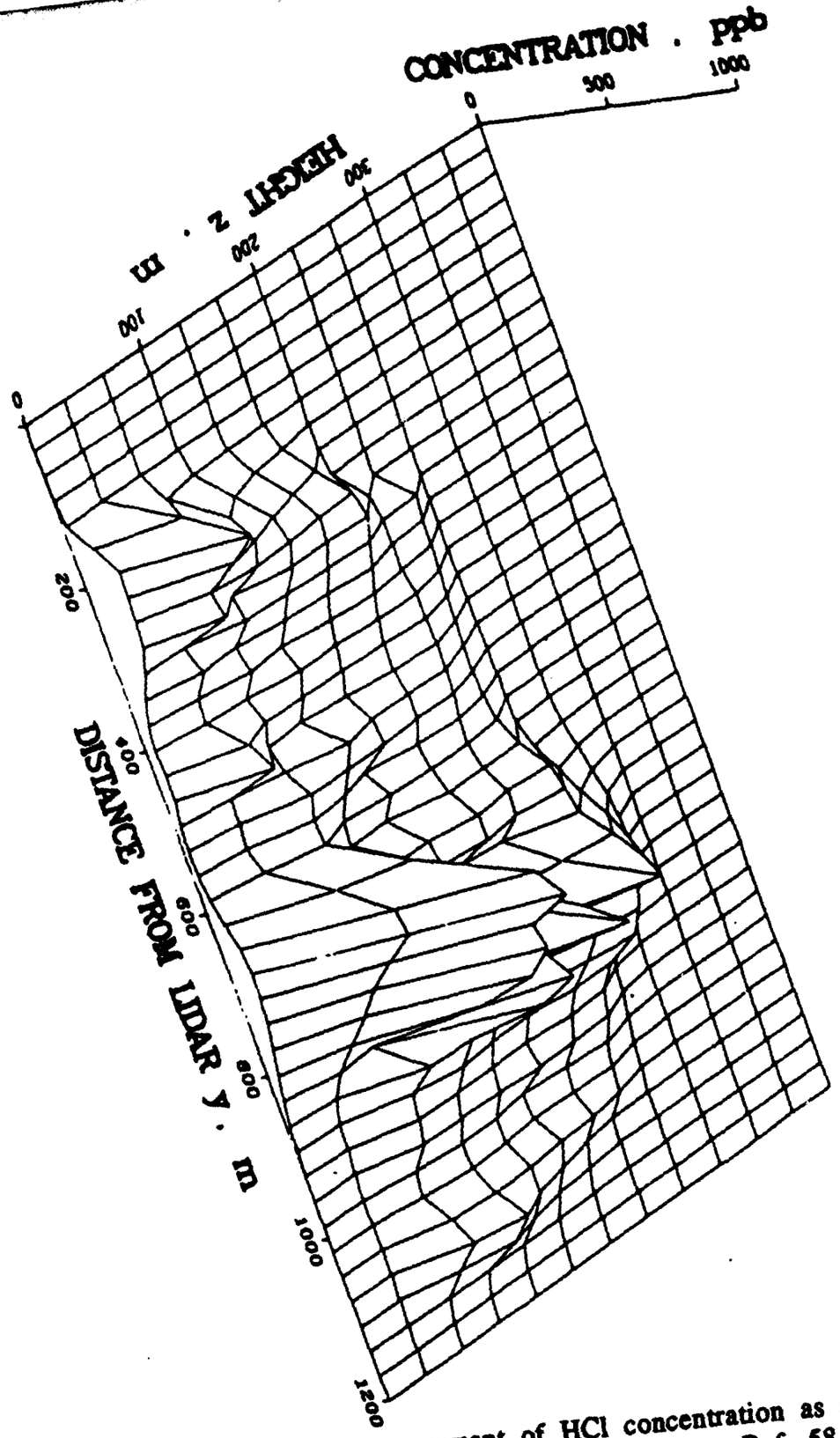

Fig. 24 — Weitkamp's measurement of HCl concentration as a function of distance from an incineration ship, taken from Ref. 58.